

Limits from the Hubble Space Telescope on a Point Source in SN 1987A

Genevieve J. M. Graves^{1,2}, Peter M. Challis², Roger A. Chevalier³, Arlin Crotts⁴, Alexei V. Filippenko⁵, Claes Fransson⁶, Peter Garnavich⁷, Robert P. Kirshner², Weidong Li⁵, Peter Lundqvist⁶, Richard McCray⁸, Nino Panagia⁹, Mark M. Phillips¹⁰, Chun J. S. Pun^{11,12}, Brian P. Schmidt¹³, George Sonneborn¹¹, Nicholas B. Suntzeff¹⁴, Lifan Wang¹⁵, and J. Craig Wheeler¹⁶

ABSTRACT

We observed supernova 1987A (SN 1987A) with the *Space Telescope Imaging Spectrograph (STIS)* on the *Hubble Space Telescope (HST)* in 1999 September,

¹Department of Astronomy, UCO/Lick Observatory, University of California, Santa Cruz, CA 95064 (graves@astro.ucsc.edu)

²Harvard-Smithsonian Center for Astrophysics, 60 Garden Street, Cambridge, MA 02138

³Department of Astronomy, University of Virginia, P.O. Box 3818, Charlottesville, VA 22903

⁴Institute for Strings, Cosmology, and Astroparticle Physics, Columbia Astrophysics Laboratory, 550 West 120th Street, Mail Code 5247, New York, NY 10027

⁵Department of Astronomy, University of California, Berkeley, CA 94720

⁶Stockholm Observatory, AlbaNova, Department of Astronomy, SE-106 91, Stockholm, Sweden

⁷Department of Physics and Astronomy, 225 Nieuwland Science Hall, University of Notre Dame, Notre Dame, IN 46556

⁸JILA, University of Colorado, Campus Box 440, Boulder, CO 80309

⁹Space Telescope Science Institute, 3700 San Martin Drive, Baltimore, MD 21218

¹⁰Carnegie Institution of Washington, Las Campanas Observatory, Casilla 601, Chile

¹¹Laboratory for Astronomy and Space Physics, Code 681, NASA Goddard Space Flight Center, Greenbelt, MD 20771

¹²Current address: Department of Physics, University of Hong Kong, Pokfulam Road, Hong Kong

¹³Mount Stromlo and Siding Spring Observatories, Private Bag, Weston Creek P.O., ACT 2611, Australia

¹⁴Cerro Tololo Inter-American Observatory, Casilla 603, La Serena, Chile

¹⁵Institute for Nuclear and Particle Astrophysics, E. O. Lawrence Berkeley National Laboratory, Berkeley, CA 94720

¹⁶Department of Astronomy, University of Texas, Austin, TX 78712

and again with the *Advanced Camera for Surveys (ACS)* on the *HST* in 2003 November. Our spectral observations cover ultraviolet (UV) and optical wavelengths from 1140–10266 Å, and our imaging observations cover UV and optical wavelengths from 2900–9650 Å. No point source is observed in the remnant. We obtain a limiting flux of $F_{\text{opt}} \leq 1.6 \times 10^{-14}$ ergs s⁻¹ cm⁻² in the wavelength range 2900–9650 Å for any continuum emitter at the center of the supernova remnant (SNR). This corresponds to an intrinsic luminosity of $L_{\text{opt}} \leq 5 \times 10^{33}$ ergs s⁻¹. It is likely that the SNR contains opaque dust that absorbs UV and optical emission, resulting in an attenuation of $\sim 35\%$ due to dust absorption in the SNR. Correcting for this level of dust absorption would increase our upper limit on the luminosity of a continuum source by a factor of 1.54. Taking into account dust absorption in the remnant, we find a limit of $L_{\text{opt}} \leq 8 \times 10^{33}$ ergs s⁻¹.

We compare this upper bound with empirical evidence from point sources in other supernova remnants, and with theoretical models for possible compact sources. We show that any survivor of a possible binary system must be no more luminous than an F6 main sequence star. Bright young pulsars such as Kes 75 or the Crab pulsar are excluded by optical and X-ray limits on SN 1987A. Other non-plerionic X-ray point sources have luminosities similar to the limits on a point source in SN 1987A; RCW 103 and Cas A are slightly brighter than the limits on SN 1987A, while Pup A is slightly fainter. Of the young pulsars known to be associated with SNRs, those with ages ≤ 5000 years are all too bright in X-rays to be compatible with the limits on SN 1987A. Examining theoretical models for accretion onto a compact object, we find that spherical accretion onto a neutron star is firmly ruled out, and that spherical accretion onto a black hole is possible only if there is a larger amount of dust absorption in the remnant than predicted. In the case of thin-disk accretion, our flux limit requires a small disk, no larger than 10^{10} cm, with an accretion rate no more than 0.3 times the Eddington accretion rate. Possible ways to hide a surviving compact object include the removal of all surrounding material at early times by a photon-driven wind, a small accretion disk, or very high levels of dust absorption in the remnant. It will not be easy to improve substantially on our optical-UV limit for a point source in SN 1987A, though we can hope that better understanding of the thermal infrared emission will provide a more complete picture of the possible energy sources at the center of SN 1987A.

Subject headings: accretion, accretion disks — stars: neutron — supernovae: individual (SN 1987A)

1. Introduction

As the first Local Group supernova in the era of modern instrumentation, Supernova 1987A (SN 1987A) is at the center of the investigation into supernova explosions and their aftermath, and into the formation of compact objects; see review articles by McCray (1993) and Arnett et al. (1989). Despite the outpouring of scientific work focused on SN 1987A, the initial neutrino burst remains the only evidence for the formation of a compact object in the supernova event. No central point source has yet been detected. Using the methods described below, we have obtained an optical upper limit of $F_{\text{opt}} \leq 1.6 \times 10^{-14}$ ergs $\text{s}^{-1} \text{cm}^{-2}$, for a point source within the supernova remnant (SNR). At a distance of 51.4 kpc, assuming 35% of the emitted flux is absorbed by dust in the remnant, this corresponds to a luminosity of $L_{\text{opt}} \leq 8 \times 10^{33}$ ergs s^{-1} . This is the best available limit in this wavelength range. The best upper limits on an X-ray point source are currently the *Chandra* limit $L_X \leq 5.5 \times 10^{33}$ ergs s^{-1} in the 2–10 keV band (Park et al. 2004), and the INTEGRAL upper limit $L_X \leq 1.1 \times 10^{36}$ ergs s^{-1} in the 20–60 keV band (Shtykovskiy et al. 2004).

The remnant is located in the Large Magellanic Cloud (LMC), a satellite galaxy of the Milky Way, near the massive 30 Doradus H II region. The distance to SN 1987A is debated within the range of 50 ± 5 kpc. By comparing the observed angular diameter with models for the emission light curve of the ring, Panagia (1999) finds a distance of 51.4 ± 1.2 kpc. Mitchell et al. (2002) use spectroscopic models to fit the expanding atmosphere of the SNR, and obtain a distance modulus of 18.5 ± 0.2 , which corresponds to 50.1 ± 4.0 kpc, and is consistent with the result of Panagia (1999). In this paper, we use a distance of 51.4 kpc.

SN 1987A is the only supernova for which we have detailed observations of the region predating the supernova outburst. Based on the coordinates of the supernova, the B3I blue supergiant, Sanduleak -69°202 (Sanduleak 1969) was identified as a likely progenitor (e.g., Kirshner et al. 1987; Walborn et al. 1987; West 1987; White & Malin 1987). SN 1987A was a Type II supernova (SN II), as determined by the strong hydrogen lines in its spectrum, but unlike normal SNe II, it did not reach its maximum luminosity until $t \approx 80$ days. Moreover, its maximum luminosity was only 1/10 the typical maximum for SNe II. Subsequent modeling of this peculiar SN II (see e.g. Woosley 1988; Nomoto, Shigeyama, & Hashimoto 1987) matched the evidence with a progenitor mass of $\sim 20M_{\odot}$, corroborating the identification of the blue supergiant Sanduleak -69°202 as the progenitor. This accounts for the differences between SN 1987A and normal SNe II, which generally result from a core collapse inside a red supergiant.

One striking feature of SN 1987A is the set of ring-like structures that surround the central remnant. These rings are material ejected from the aging star that was ionized by ultraviolet (UV) photons from the supernova explosion (see Lundqvist & Fransson 1996).

The presence of rings in the SNR strongly suggests that SN 1987A is an aspherical system. This is corroborated by the polarization of light from the remnant, the shape of the ejecta, the kinematics of the debris, the “mystery spot,” and an epoch of asymmetry in the emission line profiles known as the “Bochum event.” These all indicate an aspherical shape for the supernova (Wang et al. 2002). The central ring of SN 1987A appears in *Hubble Space Telescope (HST)* images as a 1.7" by 1.2" ellipse, interpreted as a circular ring lying in the equatorial plane of the progenitor star (Crotts & Heathcote 1991). Panagia et al. (1991) give an inclination angle of $42.8^\circ \pm 2.6^\circ$, derived from the UV light curves of the ring.

The progenitor star, Sanduleak -69°202, is estimated to have had a zero-age main-sequence (ZAMS) mass $M \sim 20 M_\odot$. This mass lies in the range where it is uncertain whether core collapse will form a neutron star or a black hole. Simulations by Fryer (1999) show that both $15M_\odot$ and $25M_\odot$ stars will collapse initially to a neutron star, but that the neutron star left by the collapse of the $25M_\odot$ star will accrete gravitationally bound material and further collapse to a black hole. The mass boundary between these possible end states depends on the neutron star equation of state, the physics used in the model, and other factors. The asymmetry of the explosion also may have influenced the final outcome. With a progenitor mass of $M \sim 20M_\odot$, the compact remnant of SN 1987A could be either a neutron star or a black hole.

To date, there is no direct evidence for a compact object at the center of the SN 1987A remnant. Suntzeff et al. (1992) give an upper limit on the energy contribution from a central continuum source of 8×10^{36} ergs s^{-1} for 1500 days after outburst. The current spectrum of SN 1987A is dominated by emission lines from gas in the remnant, powered by the radioactive decay of ^{44}Ti ; see Kozma & Fransson (1998) for a detailed discussion of the line emission. Radio astronomers have been looking for a pulsar in the remnant of SN 1987A, but no pulsar has been seen. Gaensler et al. (1997) include a summary of the negative results of this search. A claim was made for a submillisecond optical pulsar in SN 1987A (Kristian et al. 1989), but it was later retracted (Kristian 1991), the false signal being attributed to electrical noise in the data acquisition system. More recently, Middleditch et al. (2000) have presented evidence for a millisecond pulsar, but their results have not been confirmed by others. Fryer, Colgate, & Pinto (1999) point out that even if such a pulsar were beamed away from our line of sight, we would expect to see a significant luminosity contribution from the surrounding debris, acting as a calorimeter.

In this paper, we place an upper limit on the luminosity from a possible continuum source in SN 1987A that is three orders of magnitude lower than previous values. We do this using recent observations of the SNR which take advantage of the high sensitivity and powerful resolution of the *Advanced Camera for Surveys (ACS)* on *HST* to probe the

remnant deeply in five filters, ranging from near-UV to near-infrared (IR) wavelengths. Our observations and data reduction are summarized in §2. We present our upper limits from the spectrum and the images in §3, and discuss the possible effects of internal dust absorption. Section 4 considers our upper limits in the case of a potential binary companion or an optical pulsar, and compares the limits on a compact object in SN 1987A with point sources in other SNRs. Various accretion models are summarized in §5 and are discussed in the context of our upper limits on a continuum source. fallback models for SNRs are described in §6, and §7 summarizes our conclusions.

2. Observations

2.1. *STIS* Observations

During the month of 1999 September, the Supernova INTensive Study (SINS) group made a series of spectral observations of SN 1987A using the *Space Telescope Imaging Spectrograph* (*STIS*) on board the *HST*. These spectra were reduced using the on-the-fly calibration system provided by the Space Telescope Science Institute. The observations covered the entire wavelength range available from *STIS*, 1140–10266 Å (Table 1). The *STIS* observations were as follows: in the far-UV with the 0.5" slit using the G140L grating; in the near-UV with the 0.5" slit and the G230L grating; in the optical with the 0.2" slit and the G430L grating; and in the optical through near-IR with the 0.2" slit and the G750L grating. The slit was oriented to cross the central region of the supernova, and to exclude two bright foreground stars located $\sim 1.3''$ away on the sky (see Figure 1). Each observation has multiple exposures and spatial dithers to remove the cosmic rays, flat-field features, and hot pixels. Additional cosmic ray cleaning was done on each individual exposure. The spectra were averaged over these multiple exposures, using a weighted median algorithm.

We used the IRAF* program *apall* to collapse the two-dimensional (2-D) spectra into one-dimensional (1-D) spectra for each grating. A compact remnant or accretion system in the SNR would appear as a point source at the center of the supernova debris, and as a continuum source along the center of the 2-D spectrum. We extracted the 1-D spectrum from the geometric center of the debris region, with a width of 4 pixels. This is the width of the point spread function (PSF) in the 2-D spectra. The flux was summed over this 4-pixel width to include the total flux from the central object. The IRAF program *scombine*

*IRAF is distributed by the National Optical Astronomy Observatories, which are operated by the Association of Universities for Research in Astronomy, Inc., under cooperative agreement with the National Science Foundation.

was used to combine the spectra from the four gratings into one spectrum spanning the wavelength range 1140–10266 Å. A steep rise is observed in the spectrum over wavelengths shorter than 1400 Å. This is probably due to noise in the far-UV data multiplied by a large flux-correction factor.

Interstellar reddening is significant in the direction of SN 1987A, so to place limits on the intrinsic properties of a source the spectrum must be corrected for this effect. The reddening in the 30 Doradus region is highly variable; Panagia et al. (2000) have calculated the reddening for over 2,000 individual stars within 30 pc of SN 1987A, and find a large spread of reddening values, with an average value of $E(B - V) = 0.203 \pm 0.072$ mag.

The best value for the reddening in the direction of SN 1987A should be the value for stars in the immediate vicinity of the SNR. We use the reddening derived by Scuderi et al. (1996) for Star 2, one of the bright stars directly adjacent to the SNR. Scuderi et al. (1996) find a total of $E(B - V) = 0.19 \pm 0.02$ mag of reddening in the direction of Star 2. They show that the observed reddening of Star 2 is well fit by a two-component reddening model, in which the Galactic reddening curve of Savage & Mathis (1979) and the Fitzpatrick (1986) reddening curve for the 30 Doradus region are combined in a ratio of 1:2. The extinction function for the 30 Doradus region derived by Fitzpatrick (1986) differs significantly from that of the Galaxy in the UV: the bump at 2175 Å is significantly weaker and flattened compared to Galactic absorption, there is greater absorption at wavelengths shorter than 2000 Å, and from there, the extinction rises steeply toward the far-UV. It also differs from the standard LMC extinction function. Following Scuderi et al. (1996), we use the Savage & Mathis (1979) reddening curve with $E(B - V)_{\text{Galactic}} = 0.06$ mag and $R_V = 3.2$ for the Galactic reddening, and the Fitzpatrick (1986) reddening curve with $E(B - V)_{\text{LMC}} = 0.13$ mag and $R_V = 3.1$ for the LMC reddening.

2.2. ACS Observations

The images were taken in 2003 November by SINS, using the *High Resolution Camera (HRC)* and *ACS* on board *HST*. We obtained images in five filters: F330W, F435W, F555W, F625W, and F814W, which correspond to the *HRC* UV, Johnson B, Johnson V, Sloan Digital Sky Survey (SDSS) r, and broad I bands respectively. These five filter bands were chosen to cover the entire wavelength range from 2900–9650 Å, spanning the near-UV to the near-IR.

The images were drizzled to combine dithered exposures and remove cosmic rays (see Fruchter & Hook 2002). These observations are summarized in Table 2, and the imaging data are shown in Figure 2. A visual inspection of the images shows that no point source is

apparent in the SNR. A quantitative upper limit based on these images will be presented in §3.2.

3. Upper Limits on the Brightness of SN 1987A

3.1. Upper Limits from the Spectrum

The spectrum of the central source in SN 1987A corrected for interstellar extinction is shown in Figure 3. To get a limit on a point source, we looked between the emission lines for the spectrum of an underlying continuum object. The spectrum is dominated by H α , Mg, Fe, O, Ca, and Na emission features in the cool gas surrounding the compact remnant ($T \approx 130\text{--}160$ K). There are also a variety of metal lines, powered by the reprocessing of radioactive decay from ^{44}Ti ; see Chugai et al. (1997) and Wang et al. (1996) for a thorough discussion of the emission spectrum of SN 1987A. Underneath this emission spectrum, there is a continuum flux density, on the order of $F_\lambda = 10^{-17}$ ergs s $^{-1}$ cm $^{-2}$ Å $^{-1}$, which corresponds to $L_\lambda = 3 \times 10^{30}$ ergs s $^{-1}$ Å $^{-1}$ at a distance of 51.4 kpc. This continuum flux could include flux from weak emission lines, continuum radiation from the gas in the SNR, continuum emission from a compact object in the center of the remnant, or very likely a combination of emission from all of these sources. Our measurement of this continuum flux from SN 1987A places an upper limit on the contribution from a compact object.

In our continuum fit, we used only the wavelength ranges that lie *between* conspicuous emission lines: 1920–2070 Å, 3875–4020 Å, 4615–4665 Å, 5405–5575 Å, 6010–6210 Å, 6780–7080 Å, 7555–8060 Å, 8925–9125 Å, 9400–9620 Å, 9830–9980 Å, and 10100–10150 Å.

We fit a polynomial function to these regions of the spectrum. The continuum fit is plotted with the spectrum in Figure 3 as the green dashed line. We found that a seventh-order Chebyshev polynomial gave the best fit. We then integrated this function across the spectrum to obtain an upper limit on the total luminosity of the central source. In the optical range covered by our imaging data (2900–9650 Å) the integrated continuum flux was found to be 5.9×10^{-14} ergs s $^{-1}$ cm $^{-2}$. At 51.4 kpc, this corresponds to an upper limit on the optical luminosity of $L_{\text{opt}} \leq 1.9 \times 10^{34}$ ergs s $^{-1}$, roughly five times the optical luminosity of the Sun. In the UV range (1400–2900 Å) the integrated continuum flux was 5.5×10^{-14} ergs s $^{-1}$ cm $^{-2}$, therefore $L_{\text{UV}} \leq 1.7 \times 10^{34}$ ergs s $^{-1}$.

3.2. Upper Limits from Images

We examined *ACS* images of SN 1987A taken in 2003 November to determine an upper limit on a point source in the SNR. We approached this task by asking how bright a point source in the center of the debris could elude detection. We determined the geometric center of the remnant in several different ways: by fitting an ellipse to the inner ring of the SNR, by fitting a circular aperture around the central debris, and by eye. These measurements all agreed within two pixels. For observations made with *HRC*, the pixel size varies across the detector from $\sim 0''.0275$ to $0''.0287$ on a side (Mack et al. 2003). Using a pixel size of $0''.028$ per pixel, a two pixel uncertainty in the centerpoint of the remnant corresponds to $0''.056$. Even if the supernova explosion imparted a kick velocity of 1000 km s^{-1} to the compact object, it would only have travelled a maximum of $0''.07$ on the sky by the time of our observations, or 2.5 pixels. Allowing for a high initial kick velocity and a two-pixel uncertainty in the centerpoint of the remnant, we can draw a circle in the center of the remnant with a radius of 4.5 pixels ($0''.126$) that should contain any compact object resulting from the supernova event. This 4.5 pixel ring is shown as the red ring in Figure 2f.

If a point source exists within the remnant, it must be too dim to be detected by visual inspection. This depends both on the flux from the source and how it hits the detector; if most of the light from the point source falls on one pixel in the detector, it will be more easily visible against the glowing debris in the center of the remnant than if the point source falls between pixels and its light is distributed over as many as four pixels. The point spread functions (PSFs) of actual sources in each image should give a reasonable sampling of this effect. To determine the brightest point source that could hide within the remnant, we used the software package *DAOPHOT* (Stetson 1987) to do photometry on the entire field in each image, producing a photometry catalog of around 1,800 sources for each imaging band. We then inserted actual PSFs of field stars with a 3-pixel radius into the central debris of SN 1987A, at the centerpoint shown by the red dot in Figure 2f. The insertion was done using a pixel-by-pixel substitution of the PSF into the central debris. For each pixel within a 3-pixel radius of the central point, the count level of the PSF pixel was compared with the count level of the corresponding pixel in the central debris, and the brighter pixel was placed in the artificial image. This has the effect of inserting the full radius of the PSF into the central debris, without creating a dark ring around the central PSF.

Starting with bright sources that were clearly visible, we inserted progressively fainter objects until we were unable to detect the inserted source, repeating the process for each imaging band. Figure 4 shows this process for the B-band filter (F435W). The *DAOPHOT* catalog gave the total counts for the limiting objects, measured in a 4-pixel aperture. We used aperture corrections derived from white dwarfs in the image to correct to an infinite aperture,

giving us the total counts of the brightest point source that could remain undetected in SN 1987A.

To test the robustness of this result against the uncertainty in the centerpoint and the movement of a compact remnant due to an initial kick velocity, we repeated the measurement in each filter at four other points within the 4.5 pixel ring shown in Figure 2f. In four of the five filters, the measured upper limits were within 5% of the original results for all measured locations in the 4.5 pixel ring. In filter F555W, the measured upper limit varied by as much as 14% between the various measured locations. In §3.3, we will show that dust absorption within the remnant is likely to raise our upper limit by a factor of 1.54 (54%), thus the uncertainties due to dust absorption are several times larger than the uncertainties due to the centerpoint determination and the movement of the remnant due to an initial kick velocity.

To convert the measured counts to physical flux units, we assumed a flat spectrum across each imaging band. We then used the IRAF package *synphot** to convert a count level into a constant flux per angstrom (F_λ) for each filter.

In detail, we did this using the *synphot* task *calcphot* to compute the total counts produced by an input spectrum. The spectrum was specified as a flat spectrum with constant F_λ . At this stage, we also included a correction for the reddening due to dust in the LMC and our Galaxy. As in section 2.1, we used an $E(B - V)_{\text{Galactic}} = 0.06$ mag with $R_V = 3.2$ for the Galactic foreground reddening and $E(B - V)_{\text{LMC}} = 0.13$ mag with $R_V = 3.1$ for the reddening contribution from the LMC. We used the Savage & Mathis (1979) reddening curve for the Galactic reddening, and the Howarth (1983) LMC reddening curve provided in the *synphot* task *calcspec*. In this case, the difference in the reddening between the Howarth LMC curve and the Fitzpatrick curve specific to the 30 Doradus region is irrelevant, because it does not affect the wavelength range covered by our imaging (2900–9650 Å).

The flat spectrum, corrected for reddening, was used as the input spectrum for *calcphot*, and the constant flux level F_λ was varied until the output count level matched our upper limit on total count level for a point source in each filter. The upper limits for each filter are given in Table 3. The value of F_λ for each filter was used over the entire filter width, as defined by the “applied filter width” in Table 3. The applied filter width for each filter was chosen so that there were no gaps between filters. The transition wavelengths between adjacent filters were determined by the wavelengths at which the *ACS/HRC* filter throughput curves crossed. This means that at all wavelengths in the 2900–9560Å range, the corresponding value of F_λ

**Synphot* is a part of the software product STSDAS. STSDAS is a product of the Space Telescope Science Institute, which is operated by AURA for NASA.

is that belonging to the filter with the highest throughput value for that wavelength. For comparison, the upper limit on F_λ for each filter is plotted against the 1999 *STIS* spectrum in Figure 3 as a thick solid line, whose color corresponds to the color of the filter (violet for UV-band, blue for B-band, yellow for V-band, red for R-band, and maroon for I-band). All of the upper limits from the imaging data lie below the continuum fit to the spectrum, so the 2003 November imaging data give a lower limit than the 1999 September spectroscopic data. The extracted spectrum includes more background than the *ACS* images, which use the full resolution of the *HST*.

To obtain a total optical luminosity limit, the flux density per Angstrom F_λ for each filter was integrated across the applied filter width, then the contributions from each filter were summed. The summed flux was converted to an upper limit on the total optical flux from a point source in the remnant of SN 1987A: $F_{\text{opt}} \leq 1.6 \times 10^{-14}$ ergs s⁻¹ cm⁻². At a distance of 51.4 kpc, this corresponds to an intrinsic luminosity of $L_{\text{opt}} \leq 5 \times 10^{33}$ ergs s⁻¹. This is comparable to the optical luminosity of the Sun, and is three orders of magnitude lower than any previously published upper limit for this source.

3.3. The Effects of Dust Absorption

By about 650 days after the first detection of SN 1987A, most of the bolometric luminosity of the SN was being emitted in the IR. This has been interpreted as radiation from dust that condensed within the SNR. Dust began to form as early as day 100 and the formation of new dust appears to have dropped dramatically after day 650 (Bouchet & Danziger 1993). There is no evidence for spectral reddening due to the dust in the SNR, which suggests that the dust is opaque “black dust” made of particles that are large compared to the wavelength of these observations.

An analysis of data across the IR bands by Bouchet et al. (1996) shows that 97% of the bolometric luminosity of SN 1987A was being emitted in the IR at day 2172. Since that energy is initially emitted at higher wavelengths, dust absorption has a significant effect on the UV and optical luminosity of the SNR. To determine the effects of dust on our upper limit, we will assume that 97% of the UV and optical luminosity of SN 1987A was being absorbed by dust at day 2172. A substantial portion of the observed IR luminosity may be due to collisional heating, rather than the re-absorption of UV or optical radiation, so the attenuation may be less than 97%.

An attenuation of 97% at day 2172 corresponds to an effective optical depth of $\tau_{\text{eff}} = 3.5$. This is equivalent to the mean optical depth, if the dust is distributed uniformly. However,

there is evidence that some significant portion of the dust is in clumps (Bouchet & Danziger 1993; Bouchet et al. 1996). Using the extinction model by Natta & Panagia (1984) for dust clumps in a Poisson distribution,

$$\tau_{\text{eff}} = N(1 - e^{-\tau_c}), \quad (1)$$

where N is the number of absorbing clumps along the line of sight and τ_c is the optical depth of the individual clumps. In the limit of opaque dust clumps, $\tau_c \rightarrow \infty$ and $\tau_{\text{eff}} \rightarrow N$.

With dust formation dropping off precipitously after day 650, it seems reasonable to assume that dust has neither been formed nor destroyed since Bouchet’s observations on day 2172. In this case, the optical depth should scale as the column density of the expanding dust cloud, that is as $1/t^2$ for homologous expansion. Scaling from day 2172 to our imaging data at about day 6110, we have an optical depth of $\tau_{\text{eff}} = 0.44$ for uniformly distributed dust. In the clumped dust scenario, with $\tau_{\text{eff}} \rightarrow N$, the optical depth also scales as the column density, and both configurations of dust in the envelope give the same value for the optical depth, $\tau_{\text{eff}} = 0.44$. This value of τ_{eff} corresponds to an attenuation of $\sim 35\%$, so dust in the remnant may be absorbing 35% of the UV and optical luminosity of SN 1987A. The actual UV and optical luminosity of the central source is likely to be 1.54 times the limit we have measured, if the dust is uniform, or clumped on small scales.

This argument for the effective optical depth for clumped dust only applies if the dust is clumped on scales that are smaller than the size of the central source that it obscures. In the worst case scenario, there would be a single, large clump of dust directly along the line of sight to the central part of the SNR. In this case, the expansion of the SNR would not thin out the dust, and the clump would have the same size and optical depth that it had at day 2172, absorbing 97% of the UV and optical flux from the central source. Again, this is based on the assumption that the observed IR flux at day 2172 was entirely due to the re-absorption of UV and optical radiation from the central source, neglecting collisional heating. This 97% attenuation corresponds to an upper limit on the optical and UV flux from SN 1987A that is ~ 30 times the limit we have measured. While this worst case scenario for dust absorption must be considered a possibility, it should not prevent us from exploring the physical implications of our upper limit in the more likely case of absorption by uniform dust, or dust clumped on small scales. Throughout the remainder of this paper, we will use an upper limit corrected for absorption at the level of 35%, as in the uniform or clumped dust scenarios described above. This results in an optical upper limit $L_{\text{opt}} \leq 1.54 \times (5 \times 10^{33})$ ergs s^{-1} , or $L_{\text{opt}} \leq 8 \times 10^{33}$ ergs s^{-1} .

3.4. Can Infrared Observations Help?

Bouchet et al. (2003) observed SN 1987A with the Thermal-Region Camera and Spectrograph (T-ReCS) on Gemini South and resolved a point source at $10\mu\text{m}$. This source corresponds to the central ejecta of the remnant, inside the inner ring. According to Fransson & Kozma (2002), 6000 days after outburst, the radioactive decay of ^{44}Ti should still be injecting enough energy into the SN ejecta to power a luminosity of 10^{36} ergs s^{-1} . The energy of this decay is enough to power the mid-IR flux observed by Bouchet et al. (2003). Assuming 10^{36} ergs s^{-1} of thermal radiation, they constrain the temperature of the dust in the ejecta to $90 \leq T \leq 100$ K. No energy source other than ^{44}Ti is needed to account for the mid-IR flux of the ejecta. Spectroscopic observations of the ejecta with the Infrared Spectrograph on the *Spitzer Space Telescope* might be able to determine the energy mechanism producing the observed mid-IR emission of the central ejecta, and either confirm ^{44}Ti decay as the energy source, or reveal the need for another contributing energy source.

4. Observed Limits Applied to Possible Continuum Sources

4.1. Possible Binary Companion

A number of evolutionary models have been proposed for SN 1987A that model the progenitor star as a member of a binary system. The earliest of these models were those of Joss et al. (1988), Fabian & Rees (1988), and Podsiadlowski (1989), followed by de Loore & Vanbeveren (1992), and others. A more recent simulation by Collins et al. (1999) models the circumstellar nebula and ring structure of SN 1987A by supposing a merger between the progenitor of SN 1987A and a binary companion before the supernova explosion.

If a companion star remains in the SNR, it would have to fit below our upper limit to escape detection. We have an upper limit $L_{\text{opt}} \leq 8 \times 10^{33}$ ergs s^{-1} , or $L_{\text{opt}} \leq 2L_{\odot}$. This restricts a surviving main-sequence companion to stars of type F6 or later, if there is clumped dust in the remnant. Our limit would also, of course, be consistent with the presence of a white dwarf companion.

4.2. Comparison with Other Point Sources in SNRs

It is instructive to compare X-ray and optical limits on SN 1987A with point sources found in other SNRs. Chakrabarty et al. (2001) identify four types of X-ray point sources that may be associated with SNRs. These are classical pulsars, anomalous X-ray pulsars

(AXPs), soft gamma repeaters (SGRs), and a catch-all category for non-plerionic X-ray point sources that do not appear to fit in any of the previous three categories. Of the classical pulsars, the ones of most interest with respect to SN 1987A are the young pulsars. Table 4 shows X-ray and optical luminosities for a number of other point sources detected in SNRs. The table combines data taken from Table 3 of Chakrabarty et al. (2001) and Table 2 of Zavlin & Pavlov (2004b), as well as some additional optical upper limits. The table includes only point sources that appear to be associated with SNRs.

From Table 4, we can see that the X-ray and optical upper limits on the luminosity of a central source in SN 1987A are low enough to present an interesting comparison with other point sources in SNRs. Of the young pulsars listed in Table 4, only those with ages $> 1 \times 10^4$ yr are consistent with the limits for SN 1987A. Standard models for pulsars give a declining pulsar power with age, making the case for a pulsar in SN 1987A problematic. The youngest of the young pulsars are all too bright in X-rays to fit within the X-ray limits. In fact, all of the sources listed in Table 4 which are consistent with the limits on SN 1987A have ages ≥ 5000 yr, with the exception of Pup A; a source such as Pup A could remain hidden in the central debris of SN 1987A. It should be noted however that the age given in the table for Pup A, 3000 years, is derived from the kinematics of fast moving oxygen filaments in the remnant. Ages derived from the X-ray temperature are 5000-10,000 yr (see Winkler & Kirshner 1985), so there is significant uncertainty in this result. Overall, this comparison shows that any point source in the remnant of SN 1987A would have to be fainter than the X-ray point sources detected in other very young supernova remnants.

4.3. A Pulsar in SN 1987A?

Since its outburst, astronomers have been looking for a pulsar in the remnant of SN 1987A as confirmation of the widely-accepted theory that pulsars are born in supernovae. Despite repeated observations, no radio pulsar has been detected to date. The paper by Gaensler et al. (1997) includes a summary of the negative results of this search. The observations in Gaensler et al. (1997), taken with the Australia Telescope Compact Array (ATCA), show an asymmetric shell of radiation around the stellar remnant, but no central point source. The lack of a central radio source and radio pulsations is evidence against the presence of a radio pulsar.

Middleditch et al. (2000) report optical timing observations that may imply the existence of an optical pulsar in the remnant of SN 1987A with a period of 2.14 ms. Their data were taken between 1992 and 1996 on multiple telescopes, including those at the *European Southern Observatory (ESO)* and the *HST*. The signal is detected sporadically on all of the

instruments, with a signal detected in 21 out of the 78 nights of observing.

To escape detection in optical images of SN 1987A, a potential pulsar would have to have either a small dipole magnetic field, or a very large one. Ögelman & Alpar (2004) use a previous upper limit on the bolometric luminosity of SN 1987A to constrain the properties of a pulsar in the remnant. They show that an upper limit on the luminosity constrains the initial rotation period P_0 and the magnetic dipole moment μ such that there is an elliptical region of P_0 - μ space that is excluded as possible values for a pulsar in SN 1987A. Using data from Soderberg, Challis, & Sontzeff (1999), they derive a limit $L_{\text{bol}} \leq 3 \times 10^{34}$ ergs s^{-1} at $t = 11.9$ years. The corresponding ellipse in P_0 - μ space excludes the range of “normal” magnetic dipole moments for the observed range of typical pulsar periods. This means that a young pulsar in the remnant of SN 1987A must have either a weak magnetic dipole moment or a very strong magnetic dipole moment, pushing it into the range of a magnetar. For a pulsar with an initial period of 0.03 seconds (\sim the Crab pulsar), Ögelman & Alpar (2004) find that the magnetic field is limited to $\mu < 2.5 \times 10^{28}$ Gauss cm^3 , or $\mu > 2.4 \times 10^{34}$ Gauss cm^3 . For the pulsar claimed by Middleditch et al. (2000) with a period of 2.14 ms, they find the magnetic field is $\mu < 1.1 \times 10^{26}$ Gauss cm^3 or $\mu > 2.4 \times 10^{34}$ Gauss cm^3 . These values are outside the bounds of normal pulsars. For comparison, conventional pulsars have magnetic moments of $\sim 10^{30}$ Gauss cm^3 .

If a pulsar in SN 1987A were shrouded in thick dust, the dust would act as a calorimeter, reradiating energy beamed into it by the pulsar. This would appear as IR flux from the central ejecta. Bouchet et al. (2003) observe a mid-IR luminosity of $\approx 10^{36}$ ergs s^{-1} . This is consistent with the IR luminosity assumed by Ögelman & Alpar (2004), therefore their conclusions would apply even in the case where dust is obscuring more than 97% of the pulsar luminosity and reradiating the energy in the infrared.

Based on the arguments presented here, and also upon the comparison with other young pulsars, it seems unlikely that the remnant of SN 1987A currently harbors a pulsar. Theoretical models of pulsar formation (ie. Blandford, Applegate, & Hernquist 1983) give formation times for pulsars of up to 10^5 yr, so it may be that a pulsar has not yet had time to form in the remnant.

5. Accretion Models

5.1. Overview of Accretion

In the aftermath of a supernova, models predict a certain amount of fallback, in which gravitationally bound debris from the explosion eventually accretes onto the compact object

at the center. For SN 1987A, the amount of matter that accretes onto the central object during fallback was estimated by Chevalier (1989) to be $M_{\text{acc}} \approx 0.15M_{\odot}$. He assumes spherical accretion, in which the amount of fallback is strongly dependent upon the sound speed c_s of the gas in the remnant; the accretion rate \dot{M}_{acc} scales as $\dot{M}_{\text{acc}} \propto c_s^{-3}$ (Chevalier 1989). More recent papers on fallback accretion around neutron stars use a value of $M_{\text{fallback}} \leq 0.1M_{\odot}$ (Chatterjee, Hernquist, & Narayan 2000). In either case, accretion could be significant and might power a central source. In the following sections, we will examine possible accretion scenarios for the central source in SN 1987A.

There are two widely-recognized accretion regimes: a viscous, differentially rotating flow in which matter loses energy through viscous friction and spirals in toward the central object, and a spherically symmetric accretion flow. For a viscous differentially rotating flow, there are four known self-consistent solutions to the equations of hydrodynamics, summarized by Narayan, Mahadevan, & Quataert (1998). Of these, only two need concern us. The first is the famous solution of Shakura & Sunyaev (1973), in which accretion occurs through a geometrically thin, optically thick disk that radiates everywhere as a blackbody, with a temperature gradient throughout the disk. There are two solutions in the form of advection-dominated accretion flows (ADAFs), one for optically thick gas inflow, and one for optically thin, low-density inflow. At the accretion rates predicted by fallback models (see Figure 5), the accretion rate is too high to be optically thin. We will therefore focus on the optically thick advection-dominated accretion regime, in the form of a “slim disk” model. The fourth solution, first proposed by Shapiro, Lightman, & Eardley (1976), is self-consistent, but thermally unstable and is therefore a theoretical solution only, not expected to exist in real systems (as discussed in Narayan, Mahadevan, & Quataert 1998).

5.2. Spherical Accretion

In the absence of significant angular momentum, fallback from the supernova explosion would form a spherical cloud of debris moving radially toward the central object. Some models of fallback for SN 1987A assume spherically symmetric accretion (Chevalier 1989; Houck & Chevalier 1991; Brown & Weingartner 1994). Chevalier (1989) also suggests that there are phases in the accretion process where pressure effects can be neglected, resulting in a ballistic flow.

Throughout the paper, we will parameterize the accretion rate as

$$\dot{m} \equiv \left(\frac{\dot{M}}{\dot{M}_{\text{Edd}}} \right), \quad (2)$$

where \dot{M}_{Edd} is the Eddington accretion rate given by

$$\dot{M}_{\text{Edd}} \equiv \frac{L_{\text{Edd}}}{\eta_{\text{eff}} c^2}, \quad (3)$$

L_{Edd} is the Eddington luminosity, and η_{eff} is the efficiency with which gravitational energy is released. For an object with mass M that is accreting hydrogen gas,

$$L_{\text{Edd}} = 1.30 \times 10^{38} \left(\frac{M}{M_{\odot}} \right) \text{ ergs s}^{-1}. \quad (4)$$

The dimensionless luminosity is

$$l = \left(\frac{L}{L_{\text{Edd}}} \right). \quad (5)$$

Using the value of the efficiency $\eta_{\text{eff}} = 0.1$ as given in Frank, King, & Raine (1992) and equation (3), the Eddington mass accretion rate is

$$\dot{M}_{\text{Edd}} = 2.2 \times 10^{-8} \left(\frac{M}{M_{\odot}} \right) M_{\odot} \text{ yr}^{-1}. \quad (6)$$

Houck & Chevalier (1991) use spherical accretion to model neutron-star accretion in SNRs, and then apply their results to SN 1987A. Brown & Weingartner (1994) follow the derivation for SN 1987A of Chevalier (1989), with the modification of including the neutrino-cooling function derived by Houck & Chevalier (1991). They address scenarios for both neutron-star and black-hole accretion. Brown & Weingartner estimate that fallback material on the order of 10^{-4} – $10^{-3} M_{\odot}$ will remain in the vicinity of the central compact object, after the first 2–3 years of steady accretion. This material will accrete onto the central object within the next ~ 10 – 10^3 years (Houck & Chevalier 1991).

If the central object is a neutron star, the accreting matter will eventually radiate some significant fraction of its rest energy. Assuming 10% radiative efficiency, $10^{-4} M_{\odot}$ accreting over ~ 4000 years will result in radiation on the order of the Eddington luminosity, $L_{\text{Edd}} = 1.82 \times 10^{38} \text{ ergs s}^{-1}$, four orders of magnitude higher than the observational upper limits. Dust or no dust, the remnant of SN 1987A does not harbor a spherically accreting neutron star.

For a black hole, there are mechanisms by which material can accrete with efficiencies $\ll 0.1$, so accretion at the rate discussed above does not necessarily lead to Eddington luminosities. After the initial 2–3 years of neutrino-dominated steady accretion, the only energy able to escape the black-hole system is that produced by the compression work done on the infalling material before it crosses the photon trapping radius of the black hole. Brown & Weingartner (1994) show the trapping radius to be $r_{\text{tr}} = 0.6 R_m$. Inside this radius, the

time it takes a photon to diffuse outward is larger than the timescale for advection toward the central object, therefore most of the radiation would be advected inward and could not escape. Photon advection results in luminosities on the order of $L \approx 10^{34}$ – 10^{35} ergs s⁻¹ for accretion rates as high as $\dot{m} = 10^4$. The optical limit for SN 1987A at the time of their paper was $L_{\text{opt}} \leq 6 \times 10^{36}$ ergs s⁻¹, too high to constrain potential black-hole radiation.

More recently, Zampieri et al. (1998) have presented both an analytic analysis and a simulation using a radiation hydrodynamic Lagrangian code to determine the luminosity produced by a black hole undergoing spherical accretion. Their analytic result is derived by combining the work of Colpi, Shapiro, & Wasserman (1996), who solve the equations of hydrodynamics for a fluid accreting onto a stellar remnant from a reverse shock wave, with the Blondin (1986) model of hypercritical spherical accretion. Applying parameters for SN 1987A given by Chevalier (1989), they find

$$l = \frac{8 \times 10^{-3}}{(M_{\text{BH}}/M_{\odot})^{1/3} [t(\text{yr})]^{25/18}}, \quad (7)$$

in units of the Eddington luminosity. When the accretion is optically thick, as modeled here, the numerical simulations run by Zampieri et al. show both the effective temperature T_{eff} and the temperature of the gas in the photosphere T_{ph} to have values in the range of $\sim 8,000$ – $10,000$ K, producing a roughly blackbody spectrum. These temperatures would produce blackbodies with peaks in the visible to near-UV range, so most of the radiation should fall within the range we have observed. The numerical models of Zampieri et al. (1998) are in agreement with the above analytical result to within $\sim 30\%$. We will take this value as an estimate of the uncertainty in the model.

At the time corresponding to our data, $t = 16.75$ years, we find that $l = 1.40 \times 10^{-4}$, or $L_{\text{acc}} = 2.72 \times 10^{34}$ ergs s⁻¹. Our upper limit, accounting for 35% dust absorption, is $L_{\text{opt}} \leq 8 \times 10^{33}$ ergs s⁻¹. This is about 1/3 the luminosity predicted by the (Zampieri et al. 1998) calculation.

Their calculation is based on a black hole with mass $M = 1.5M_{\odot}$. It is not clear that black holes form with such low masses. Estimates for the lowest possible mass of a black hole range between $1.5M_{\odot}$ and $2.5M_{\odot}$; see Zampieri et al. (1998) for a list of these models. The corresponding accretion luminosity for a black hole with a mass of $2.5 M_{\odot}$ is $L_{\text{acc}} = 3.8 \times 10^{34}$ ergs s⁻¹. Zampieri et al. (1998) use the lowest hypothesized mass limit on a black hole. Also, Blondin (1986) gives his hypercritical accretion model as a minimum value for the accretion-produced luminosity, based upon the assumption that the only mechanism for accretion-produced luminosity is the compression of the material outside of the trapping radius. The calculations of Zampieri et al. (1998) produce conservatively low values of accretion radiation, both in the choice of black-hole mass ($M = 1.5M_{\odot}$) and in the assumption that compression

of the material outside the trapping radius is the only mechanism for accretion radiation; hence, their result should be a lower limit on the accretion luminosity.

The lower limit predicted by the Zampieri et al. (1998) model for a $1.5 M_{\odot}$ black hole undergoing accretion is more than 3 times larger than our upper limit on a point source in SN 1987A. In the case of large amounts of dust absorption ($\geq 80\%$), a spherically accreting black hole could be concealed within the remnant of SN 1987A, but in the case of more moderate dust absorption, this picture conflicts with the observations.

5.3. Spherical Accretion with Large Iron Opacity

Fryer, Colgate, & Pinto (1999) have done fallback accretion modelling in which iron opacity plays an important role in suppressing accretion. As the temperature of the remnant decreases, neutrino cooling falls off and the radiation is dominated by photon transport. When the outer layers of the atmosphere reach the temperature $T = 0.2$ keV, the iron opacity in the model atmosphere increases by a factor of 300 and dominates over electron scattering. The iron opacity they model can be as much as 3–4 orders of magnitude greater than the opacity caused by Compton scattering, which leads to suppression factors of $L_{\text{Edd,Fe}}/L_{\text{Edd,e}^-} = 10^{-2.5} - 10^{-3.9}$. For singly-ionized, iron-group-rich material, they use an Eddington limit of

$$\begin{aligned} L_{\text{Edd,e}^-} &= 1.25 \times 10^{38} \left(\frac{M}{M_{\odot}} \right) \frac{\bar{A}}{f} \text{ ergs s}^{-1} \\ &\approx 7 \times 10^{39} \left(\frac{M}{M_{\odot}} \right) \text{ ergs s}^{-1}, \end{aligned} \quad (8)$$

where \bar{A} is the mean atomic weight of the material, and f is the mean number of free electrons per ion.

With the Eddington limit suppressed by iron opacity, the opaque outer layer of the atmosphere prevents higher rates of radiation. The gravitational energy in the photons inside this outer layer cannot escape efficiently, and most of the energy goes into ejecting mass from the system, creating a photon-driven wind that pushes the outer portions of the atmosphere away from the stellar remnant while the inner atmosphere is accreted onto the star at the iron opacity accretion rate. Fryer, Colgate, & Pinto (1999) compute the iron opacity Eddington luminosity at late times for several values of atmosphere density, by applying these values of the suppression factor to the Eddington limit for singly-ionized iron-rich material. By 5000 days (13.7 years) past the SN explosion, they find the iron opacity Eddington luminosity levelling off. Extrapolating the curves shown in their Figure

8 to the time of our observations at day 6110, we find $L_{\text{Edd,Fe}} = 2.0 \times 10^{36} - 1.5 \times 10^{37}$ ergs s^{-1} for densities in the range $10^{-8} \leq \rho \leq 10^{-6}$ g cm^{-3} . These values are 2–3 orders of magnitude higher than our upper limit, and are therefore inconsistent with the observations. If this model is relevant for SN 1987A, the photon-driven wind must have removed the entire envelope of accreting material on a timescale of less than 12 years, the time of our spectral observations.

5.4. Thin Disk Models

Spherically symmetric accretion may not be the best approximation of accretion onto the core of SN 1987A. The ring structures, polarization, shape of the debris and other aspects of the explosion all indicate a special axis that could be an axis of rotation (Wang et al. 2002). If there is a significant amount of angular momentum in the infalling material, the matter will settle into a geometrically thin disk, with each part of the disk orbiting the central source in a Keplerian orbit.

In systems where the timescale of external change (i.e., the mass infall) is greater than the timescale of viscosity spreading within the disk, the accreting matter settles into a steady-state disk. Steady-state disks are modeled to have a viscous dissipation flux $D(R)$ that does not depend on the local viscosity of the disk, but only on the mass of the central object M , and the accretion rate \dot{M} , as given in Shakura & Sunyaev (1973):

$$D(R) = \frac{3GM\dot{M}}{8\pi R^3} \left[1 - \left(\frac{R_*}{R} \right)^{1/2} \right], \quad (9)$$

where R_* is the radius of the neutron star. If we make the assumption that the disk is optically thick in the z -direction, the disk will radiate as a series of concentric blackbody rings, each with an effective temperature given by the standard blackbody relation, $\sigma T^4 = D(R)$, and

$$T(R) = \left\{ \frac{3GM\dot{M}}{8\pi R^3 \sigma} \left[1 - \left(\frac{R_*}{R} \right)^{1/2} \right] \right\}^{1/4}. \quad (10)$$

Therefore the flux per unit wavelength radiated from the disk is given by integrating the blackbody surface flux over the surface area of the disk,

$$F_\lambda = \int_{R_{\min}}^{R_{\max}} \frac{2\pi hc^2}{\lambda^5} \left[\frac{1}{\exp[hc/\lambda kT(R)] - 1} \right] 4\pi R dR. \quad (11)$$

We computed the flux from a thin disk by approximating a thin accretion disk as a set of concentric blackbody rings of constant temperature, using the temperature determined by equation (10). We integrated across the disk surface to compute the flux at each wavelength, and then produced a model spectrum for the disk. We took the inner radius of the disk to be the radius of a neutron star (that is, $R_{\min} = 1 \times 10^6$ cm), the mass of the central object to be $M = 1.4M_{\odot}$, and the distance to the object to be 51.4 kpc. The model spectra were reddened as in §3.2 and converted to a total count level using the *synphot* task *calcspec*. The total counts were then compared to the upper limit from §3.2 for each filter to determine which disks could hide in the SNR.

Because the high temperatures in the disk near the compact object produce X-ray and far-UV radiation, our model for the near-UV and optical spectrum is insensitive to the exact value of R_{\min} (values of $R_{\min} = 10$ km and $R_{\min} = 300$ km gave identical output to within 1%). As seen in equation (10) the temperature scales as $(M\dot{M})^{1/4}$, allowing the mass difference between a $1.4 M_{\odot}$ neutron star and a $1.5 M_{\odot}$ black hole to be absorbed into the computed value of \dot{M} . That is, the value of \dot{M} for a $1.5 M_{\odot}$ black hole accretion system at a given value of R_{\max} will correspond to $1.4/1.5 = 0.93$ times the value of \dot{M} for a $1.4 M_{\odot}$ neutron star system with the same R_{\max} . The model was run with varying values of the outer radius R_{\max} and the dimensionless accretion rate \dot{m} (see equation 2).

Figure 5a shows the values of R_{\max} and \dot{m} that are consistent with our upper limits in each band. The UV filter F330W (solid curve) gave the most stringent limit on R_{\max} and \dot{m} . The shaded region represents disk parameters that are excluded by our UV upper limit. From the figure, we can see that an accretion disk in the SNR is limited to small disk sizes and low accretion rates. The restrictions in R_{\max} - \dot{m} space given by other filter bands are also shown: the dotted curve is the limit from the B-band filter (F435W), the short-dashed curve corresponds to the V-band filter (F555W), the dot-dashed curve to the R-band filter (F625W), and the long-dashed curve to the I-band filter (F814W). We ran the simulation out to $R_{\max} = 1 \times 10^{12}$ cm. Beyond this point, the disk is cool and contributes only in the IR, therefore our optical constraint on \dot{m} will remain constant beyond $R_{\max} = 1 \times 10^{12}$ cm, as can be seen in Figure 5.

Any accretion disk in SN 1987A must be below the luminosity limit in all bands to escape detection. The UV-band limit is the most stringent, so we have used it to delineate the part of R_{\max} - \dot{m} space that is consistent with our upper limit. Uncertainties in the correction for interstellar reddening raise the UV-band limiting curve by at most a factor of two, and therefore do not qualitatively change our results for thin disk models.

It is worth investigating how various levels of dust absorption within the remnant change the region of R_{\max} - \dot{m} space that is consistent with our limit. Figure 5b shows the excluded

region for various levels of dust absorption. These limits are derived from the UV-band limit, since it gives the most stringent constraint. The excluded region in the case of no dust absorption is the solid curve from Figure 5a. Three other cases are shown: a system in which 35% of the flux is absorbed by dust, 70% of the flux is absorbed by dust, and 97% of the flux is absorbed by dust. Recall that 35% is the predicted amount of dust absorption based on the argument in §3.3, so this line corresponds to our upper limit of $L_{\text{opt}} \leq 8 \times 10^{33}$ ergs s⁻¹, and is the value we will use in our analysis. The case of 70% dust absorption would apply if our estimate of the internal dust absorption is off by a factor of two, and 97% absorption corresponds to the worst-case-scenario of a single opaque dust clump along the line of sight to the remnant.

For this limit to be useful, we must have some understanding of what “typical” values for R_{max} and \dot{m} are. Standard values of R_{max} for binary systems are given as $(2-8) \times 10^{10}$ cm in Bath & Pringle (1981), and of order 10^{10} cm in Frank, King, & Raine (1992). (These do not necessarily apply to accretion disks in SNRs, but will we use this range as an estimate of the typical size of an accretion disk around a stellar remnant.) For a disk of radius $R_{\text{max}} = 1 \times 10^{10}$ cm, our observations limit the accretion rate to $\dot{m} \leq 0.3$, in the case of 35% dust absorption. In §6, we will compare our limits on disk size and accretion rate to the values for R_{max} and \dot{m} predicted by fallback models.

5.5. The Slim Disk Model

Thin disk models operate under the assumption that the vertical structure of the disk can be treated separately from the radial structure, but this assumption breaks down at high (super-Eddington) accretion rates, ie. where $\dot{m} \geq 1$. Beyond a critical value of the accretion rate, the disk must have non-negligible thickness to remain in hydrostatic equilibrium. An early description of these slim disks is given in Jaroszyński, Abramowicz, & Paczyński (1980). They show that disks with super-critical accretion rates have luminosities near or above L_{Edd} which radiate predominantly in X-rays. For a central source with $M = 1.4M_{\odot}$, the critical accretion rate of Jaroszyński, Abramowicz, & Paczyński (1980) is a few times $10^{-8}M_{\odot} \text{ yr}^{-1}$, comparable to the Eddington accretion rate \dot{M}_{Edd} we defined in §5.2. In the next section, we will see that models of fallback in SNRs predict accretion rates after ~ 16.75 years of order the Eddington accretion rate, with $\dot{m} \sim 1$, as shown by the red and blue grids in Figure 5. At accretion rates this high, the assumption of a thin disk begins to break down. However, we would expect to see accretion luminosities of order $L_{\text{Edd}} \sim 2 \times 10^{38}$ ergs s⁻¹ for a slim disk with an accretion rate this high. These luminosities are 4 orders of magnitude higher than both the optical upper limits for SN 1987A derived in this paper, and the X-ray upper limit

of Park et al. (2004), therefore it appears unlikely that super-Eddington, slim disk accretion is an appropriate model for SN 1987A.

6. Fallback Models for SNRs

We have used our upper limit on the continuum flux from SN 1987A to constrain the rate of accretion onto a compact object under standard spherical, thin disk, and slim disk accretion models. It is instructive to compare these limiting rates to models for the fallback onto a SNR. In studying anomalous X-ray pulsars (AXPs), Chatterjee, Hernquist, & Narayan (2000) have developed a model for neutron-star accretion from a disk of fallback debris in the aftermath of a supernova explosion. Their model examines accretion from this “fossil disk” for various values of the magnetic field B and initial rotation period P_0 of the neutron star, and the mass of the disk M_d . They find that for some values of these parameters (specifically $B \leq 3.9 \times 10^{12}$ Gauss), no efficient accretion mechanism evolves and the neutron star becomes a radio pulsar on a timescale of ~ 100 years. For higher values of B , the accreting neutron star becomes an AXP. From a set of initial conditions, they evolve a time-dependent expression for the disk accretion rate $\dot{M}(t)$ as a function of time t from the explosion. The Chatterjee, Hernquist, & Narayan (2000) model has been used by Perna, Hernquist, & Narayan (2000; hereafter PHN) and later by Menou, Perna, & Hernquist (2001; hereafter MPH) to develop more detailed models of the fallback onto a compact object in a SNR. The two models differ in their choice of timescale for fallback. In this section, we compare the predicted fallback accretion in both of these models with the limits on \dot{m} for various accretion scenarios discussed in §5.

6.1. Fallback Models with a Steady-State Disk

Both the PHN and MPH fallback models are based on the Pringle (1974) solution to a steady-state accretion disk. They use the self-similar solution for the Pringle disk found by Cannizzo, Lee, & Goodman (1990):

$$M_d(t) = M_d(t_0) \left(\frac{t}{t_0} \right)^{-3/16}, \quad (12)$$

$$R_d(t) = R_d(t_0) \left(\frac{t}{t_0} \right)^{3/8}, \quad (13)$$

where t_0 is the timescale for disk formation, M_d is the total disk mass, and R_d is the outer radius of the disk. From equation (12) it follows that

$$\dot{M}_d(t) = -\frac{3}{16}M_d(t_0) \left(\frac{t}{t_0}\right)^{-3/16} \left(\frac{1}{t}\right). \quad (14)$$

We can use our limits for the \dot{M} and R of a thin disk from §5.4 in conjunction with the initial conditions of the disk, $M_d(t_0)$ and $R_d(t_0)$, to determine whether or not the proposed fallback models are compatible with our observed upper luminosity limit. In doing so, it is useful to have a general idea of likely values for these conditions. The total fallback material accreted onto the compact object is predicted to be $M_{\text{fallback}} \leq 0.1\text{--}0.15M_\odot$ (Chevalier 1989; Chatterjee, Hernquist, & Narayan 2000). Of this, a fraction will settle into the initial accretion disk. PHN use a value of $M_d = 0.005M_\odot$. We will take a broad range of $10^{-5}M_\odot \leq M_d(t_0) \leq 0.1M_\odot$ as a reasonable estimate for the initial mass of the accretion disk. For the initial radius, MPH argue that the fallback material originates outside of the core of the progenitor star with $R \leq 10^9$ cm. Using predictions for the angular momentum of the fallback material (from simulations by Heger, Langer, & Woosley 2000) and conserving angular momentum, they calculate Keplerian orbits in the range 10^6 cm $\leq R_d(t_0) \leq 10^8$ cm.

To use equations (12–14), we will need an expression for t_0 . This is where the PHN and MPH models differ. PHN assume that a fallback disk will form on the order of milliseconds. They use a value of $t_0 = 1$ ms, following Chatterjee, Hernquist, & Narayan (2000), whose numerical calculations show the models to be relatively insensitive to t_0 over larger timescales. MPH argue that disk formation ought to occur on the local viscous timescale, on the order of 10^3 s. Although M_d and R_d are only weakly dependent on t_0 ($M_d \propto t_0^{3/16}$ and $R_d \propto t_0^{-3/8}$), the choice of timescale turns out to be significant over the period of 16.75 years that have elapsed between the SN 1987A explosion and our observations.

6.2. The PHN Model

Using equations 13 and 14, with a characteristic timescale of $t_0 = 1$ ms, we can calculate a set of disk sizes and accretion rates predicted by the PHN model for the time of our observations, 16.75 years after outburst. The range of predicted R_{max} and \dot{m} are shown in Figure 5a as the blue grid. The vertical lines correspond to initial disk radii (from left to right) of 10^6 cm, 10^7 cm, and 10^8 cm. The horizontal lines correspond to initial disk masses (from top to bottom) of $10^{-1}M_\odot$, $10^{-2}M_\odot$, $10^{-3}M_\odot$, $10^{-4}M_\odot$, and $10^{-5}M_\odot$. We can see from Figure 5a that the PHN model is not consistent with our upper limits. If there is substantial dust absorption in the SNR ($\geq 70\%$) then the smallest and least massive initial

disks predicted by the PHN model may be consistent with our limits. In general, the PHN model predicts higher accretion rates than are compatible with our observed upper limit.

According to the Chatterjee, Hernquist, & Narayan (2000) model, neutron-star systems enter a phase in which the rapid rotation of the star’s magnetic field acts as a “propeller” that throws matter out from the surface of the star. In this scenario, matter cannot accrete onto the star. The propeller effect was first described by Illarionov & Sunyaev (1975). They define the corotation radius R_{co} as the radius at which the accretion disk rotates with the same angular frequency as the neutron star. The magnetospheric radius R_{mag} is the radius at which magnetic forces dominate over the gravitational force of the neutron star. When $R_{\text{co}} < R_{\text{mag}}$, the magnetosphere is rotating fast enough that the centrifugal force overcomes the gravitational pull of the neutron star and the accreting material is pushed outward. Although it is unclear whether the material is actually expelled from the system, or remains outside of the magnetosphere, it is unable to accrete onto the neutron star in either case (Menou et al. 1999). The propeller effect can operate in a thin-disk accretion regime, where the propeller effectively prevents any accretion, or in a spherical ADAF regime, where some matter is able to accrete along the poles of the neutron star’s rotational axis. Can the existence of a propeller around a neutron star in SN 1987A account for the low-level of accretion observed, as compared to the predicted level in PHN?

The propeller is only effective inside the magnetospheric radius of the neutron star where it prevents accretion onto the surface of the neutron star. Outside of the magnetospheric radius, the thin disk surrounding the propeller will still be able to radiate away some of the gravitational energy stored in the accretion flow. The magnetospheric radius for a neutron star is given by Frank, King, & Raine (1992) as

$$R_{\text{mag}} = 6.6 \times 10^7 B_{12}^{4/7} \dot{m}^{-2/7} \text{cm}, \quad (15)$$

where B_{12} is the magnetic field of the neutron star expressed in units of 10^{12} Gauss. Only large values of R_{mag} will affect the optical flux from the disk (recall from §5.4 that the inner portion of the disk contributes little flux in the optical band), therefore we maximize the propeller effect by choosing a large value for the pulsar magnetic field, $B = 10^{12}$ Gauss. When we repeated our thin accretion disk simulations for a $1.4M_{\odot}$ neutron star with a magnetic field of 10^{12} Gauss and an inner disk radius given by equation (15), we found that the resulting disk luminosities were comparable to those of disks without a propeller. The presence of a propeller does not substantially change the optical luminosity of a given size disk, so the accretion rate and outer radius limits we found for non-propeller systems apply to propeller systems as well. The PHN propeller cannot explain the low level of optical emission observed from SN 1987A.

6.3. The MPH Model

In the MPH model, the authors assume that the fallback material will settle into a disk on a timescale determined by the local viscous timescale. They write

$$\begin{aligned}
 t_0 &\equiv \frac{R^2 \Omega_K}{\alpha c_S^2} \\
 &\approx 6.6 \times 10^{-5} \left(\frac{T_i}{10^6 \text{K}} \right)^{-1} \left(\frac{R_d(t_0)}{10^8 \text{cm}} \right)^{1/2} \text{yr},
 \end{aligned}
 \tag{16}$$

where Ω_K is the local Keplerian angular speed, c_S is the speed of sound, and T_i is the initial temperature of the newly formed disk. This equation is based on an assumed viscosity parameter of $\alpha = 0.1$ and a compact object with $M = 1M_\odot$. A range of temperatures for young accretion disks is given by Hameury et al. (1998) as $10^4 \text{ K} \leq T_i \leq 10^6 \text{ K}$.

We can use equations (13) and (14) in conjunction with reasonable initial values for $R_d(t_0)$, $M_d(t_0)$, and T_i to compare the predictions of the MPH model with our upper limits for accretion-disk radiation as calculated in §5.4. As in §6.2, we investigated the following range of initial values for the radius, and mass of the accretion disk:

$$10^6 \text{ cm} \leq R_d(t_0) \leq 10^8 \text{ cm} \tag{17}$$

$$10^{-5} M_\odot \leq M_d(t_0) \leq 10^{-1} M_\odot. \tag{18}$$

We used an initial temperature range of

$$10^4 \text{ K} \leq T_i \leq 10^6 \text{ K}. \tag{19}$$

The ranges of predicted disk radii and accretion rates at $t = 16.75$ years after outburst are shown as the red grids in Figure 5. The solid grid is for disks with temperature $T = 10^6 \text{K}$; the darker dashed grid is for disks with $T = 10^4 \text{K}$. As before, the vertical lines are for initial disk radii (from left to right) of 10^6 cm , 10^7 cm , and 10^8 cm , while the nearly-horizontal lines are for initial disk masses (from top to bottom) of $10^{-1} M_\odot$, $10^{-2} M_\odot$, $10^{-3} M_\odot$, $10^{-4} M_\odot$, and $10^{-5} M_\odot$.

Our upper limit provides some restriction on the radius and accretion rate of a hot ($T = 10^6 \text{K}$) disk, limiting a disk in the central debris of SN 1987A to a small, disk ($R_{\text{max}} \leq 1 \times 10^{10} \text{ cm}$) with a low accretion rate. For disks with initial masses of $M \geq 0.005 M_\odot$, the disks must be even smaller ($R_{\text{max}} \leq 5 \times 10^9$). For cooler initial temperatures, disks of the

same initial radius do not grow as large as comparable disks at hotter temperatures. Only the largest and most massive of the cooler disks are restricted by our observed upper limits.

Notice that the MPH model predicts disk sizes that are smaller than the standard values of $(2\text{--}8)\times 10^{10}$ cm for accretion disks in binary systems. Disks with R_{max} larger than $\sim 1 \times 10^{10}$ cm are incompatible with our limits on \dot{m} unless they have less accretion than predicted by these fallback models. The smaller, cooler disks of the MPH model fit within our observed upper limits.

It is worth noting that the predictions of the angular momentum given in §6.1 for fallback systems may be too large. Recent simulations by Heger, Woosley, & Spruit (2004) include the effects of magnetic fields in the end stages of nuclear burning in massive stars. They find that a significant amount of angular momentum is lost through stellar winds, and that angular momentum is transferred from the core of the star outward through magnetic braking. Consequently, the material around the iron core prior to collapse has values of the specific angular momentum j that are 30–50 times lower than those found in the absence of magnetic fields. For Keplerian disk orbits, $j \approx \sqrt{GM}r$, where M is the enclosed mass of the orbit, and r is the radius of the orbit. A decrease in j by a factor of 30–50 corresponds to a decrease in the outer radius of the disk by about three orders of magnitude, giving initial disk radii of $10^3 \text{ cm} \leq R_d(t_0) \leq 10^5 \text{ cm}$. These are non-sensical values for the radius of a disk around a neutron star, since they are smaller than the outer radius of the star: $R_{NS} \sim 10$ km. For a neutron star, initial disk radii of $R_d(t_0) \sim 10^6\text{--}10^7$ cm are the smallest possible disk sizes. The low values of angular momentum predicted by Heger, Woosley, & Spruit (2004) suggest that the smallest disks are the most likely, or that an accretion disk may not form at all.

7. Conclusions

Taking advantage of the high resolution and sensitivity of *ACS/HRC* on *HST*, we have measured the lowest upper limit on the optical and near-UV luminosity to date for a point source at the center of the SN 1987A remnant. We find that the total optical flux is limited to $F_{\text{opt}} \leq 1.6 \times 10^{-14}$ ergs s⁻¹ cm⁻². The luminosity limit can be written

$$L_{\text{opt}} \leq 5 \times 10^{33} \text{ ergs s}^{-1} \times \left(\frac{D}{51.4 \text{ kpc}} \right)^2 \times \exp \left[\frac{A_V}{0.595} \right] \times \left(\frac{1}{1 - \alpha_0} \right)^{(t_0/t)^2} \quad (20)$$

where D is the distance to the supernova remnant, A_V is the actual value of the reddening in the direction of SN 1987A, t is the time since outburst, t_0 is the epoch of dust formation, and α_0 is the fraction of the luminosity that is absorbed within the remnant at time t_0 . Writing the luminosity limit in this form takes into account the effects of distance, reddening, and internal dust absorption, and of the uncertainties in the upper limit due to these effects. We have used $t_0 = 2172$ days and $\alpha_0 = 0.97$, resulting in an upper limit of $L_{\text{opt}} \leq 8 \times 10^{33}$ ergs s^{-1} for a point source in the remnant of SN 1987A at $t \approx 6110$ days.

We have also measured upper limits on a continuum source in the SNR by fitting a continuum level to the flux between emission lines in the spectrum of SN 1987A from 1999 September. The spectral data give limits on the luminosity of $L_{\text{UV}} \leq 1.7 \times 10^{34}$ ergs s^{-1} and $L_{\text{opt}} \leq 1.9 \times 10^{34}$ ergs s^{-1} . These limits are not as stringent as those derived from the more recent imaging data, suggesting that the remnant has dimmed in the intervening time. All of these limits are likely to be lower than the actual luminosity limit on a compact remnant, due to dust absorption within the SNR itself. In the worst-case scenario for dust absorption, as much as 97% of the light emitted by a central source may be absorbed by a thick clump of black dust along the line of sight to the SNR.

Based upon our observed upper limit, we find that a possible surviving binary companion to SN 1987A is limited to F6 and later stars. The limits on a point source in the SNR require a potential pulsar to have either a very weak magnetic dipole moment, or a very strong magnetic field that puts the magnetized neutron stars in the realm of magnetars. The pulsar must be fainter in X-rays than the other young pulsars with ages less than 10,000 years known to be associated with SNRs.

We have examined the available models for accretion scenarios. We find that spherical accretion onto a neutron star is ruled out by a factor of 10^4 . A spherically accreting black hole is also incompatible with our limit, unless the dust absorption exceeds 80%. We have also examined accretion scenarios in which the fallback material has significant angular momentum and forms a thin accretion disk or an optically thick slim disk. In the case of a thin disk, we have shown that the accretion disk must have a small radius to correspond with predicted values of the accretion rate \dot{m} , for either a neutron star or a black hole. The presence of a magnetized propeller does not substantially affect this result. The Menou, Perna, & Hernquist (2001) fallback model is consistent with the presence of a small disk accreting at a rate within our measured upper limit. A slim disk is incompatible with our upper limit. Other possibilities include the scenario in which photon winds have driven all the remaining fallback material out of the system, truncating accretion, as proposed by Fryer, Colgate, & Pinto (1999), or that all of the fallback material has already accreted onto the compact remnant on a timescale of less than 14 years.

Future spectroscopic observations in the mid- to far-IR with the *Spitzer Space Telescope* may provide additional data on the dust remaining in the SNR. A better determination of the mechanisms which power the $10\mu\text{m}$ radiation from the central ejecta might make it possible to determine the extent to which optical luminosity from a central source is being absorbed by dust in the remnant. Also, as the remnant expands, the dust should thin, allowing us to peer more deeply into the remnant. Over time, as the radiation from debris in the remnant grows dimmer and dust absorption declines, we will be able to place increasingly strong limits on a point source in SN 1987A. Eventually a point source may even be detected!

The authors would like to thank Thomas Matheson, Ramesh Narayan, and Saurabh Jha for helpful discussion and suggestions. Support for HST proposal number GO 09428 was provided by NASA through a grant from the Space Telescope Science Institute, which is operated by the Association of Universities for Research in Astronomy, Inc., under NASA contract NAS5-26555. RAC acknowledges support from NASA grant NAG5-13272. AVF is grateful for a Miller Research Professorship at U. C. Berkeley, during which part of this work was completed.

REFERENCES

- Arnett, W. D., Bahcall, J. N., Kirshner, R. P., & Woosley, S. E. 1989, *ARA&A*, 27, 629
- Bath, G. T., & Pringle, J. E. 1981, *MNRAS*, 194, 967
- Blandford, R. D., Applegate, J. H., & Hernquist, L. 1983, *MNRAS*, 204, 1025
- Blondin, J. M. 1986, *ApJ*, 308, 755
- Borkowski, K. J., de Kool, M., McCray, R., & Wooden, D. H. 1997, *Amer. Astron. Soc. Meet.* 191, #40.12
- Bouchet, P., De Buizer, J. M., Suntzeff, N. B., Danziger, I. J., Hayward, T. L., Telesco, C. M., & Packham, C. 2003, *ApJ*, 611, 394
- Bouchet, P., & Danziger, I. J. 1993, *A&A*, 273, 451
- Bouchet, P., Danziger, I. J., Gouiffes, C., della Valle, M., & Monetti, A. 1996, in *Supernovae and Supernova Remnants*, IAU Colloq. 145, ed. R. McCray & Z. Wang (Cambridge: Cambridge Univ. Press), 201
- Brown, G. E., & Bethe, H. A. 1994, *ApJ*, 423, 659
- Brown, G. E., & Weingartner, J. C. 1994, *ApJ*, 436, 843
- Cannizzo, J. K., Lee, H. M., & Goodman, J. 1990, *ApJ*, 351, 38
- Chakrabarty, D., Pivovarov, M. J., Hernquist, L. E., Heyl, J. S., & Narayan, R. 2001, *ApJ*, 548, 800
- Chatterjee, P., Hernquist, L. E., & Narayan, R. 2000, *ApJ*, 534, 373
- Chevalier, R. A. 1989, *ApJ*, 346, 847
- Chevalier, R. A., & Kirshner, R. P. 1978, *ApJ*, 219, 931
- Chugai, N. N., Chevalier, R. A., Kirshner, R. P., & Challis, P. M. 1997, *ApJ*, 483, 925
- Collins, T. J. B., Frank, A., Bjorkman, J. E., & Livio, M. 1999, *ApJ*, 512, 322
- Colpi, M., Shapiro, S. L., & Wasserman, I. 1996, *ApJ*, 470, 1075
- Corbel, S., Chapuis, C., Dame, T. M., & Durouchoux, P. 1999, *ApJ*, 526, L29
- Crotts, A. P., & Heathcote, S. R. 1991, *Nature*, 350, 683

- Dolphin, A. E. 2000, *PASP*, 112, 1397
- Eardley, D. M., Lightman, A. P., Payne, D. G., & Shapiro, S. L. 1978, *ApJ*, 224, 53
- Fabian, A. C., & Rees, M. J. 1988, *Nature*, 335, 50
- Fesen, R. A., Chevalier, R. A., Holt, S. S., & Tananbaum, H. 2002, in *Neutron Stars in Supernova Remnants*, ASP Conf. Series Vo. 271, ed. P. O. Slane & B. M. Gaensler (San Francisco: ASP), 305
- Fischera, J., Tuffs, R. J., & Völk, H. J. 2002a, *A&A*, 386, 517
- Fischera, J., Tuffs, R. J., & Völk, H. J. 2002b, *A&A*, 395, 189
- Fitzpatrick, E. L. 1986, *AJ*, 92, 1068
- Frank, J., King, A. R., & Raine, D. J. 1992, *Accretion Power in Astrophysics* (Cambridge: Cambridge Univ. Press)
- Fransson, C., & Kozma, C. 2002, *New Astronomy Reviews*, 46, 487
- Fruchter, A. S., & Hook, R. N. 2002, *PASP*, 114, 144
- Fryer, C. L. 1999, *ApJ*, 522, 413
- Fryer, C. L., Colgate, S. A., & Pinto, P. A. 1999, *ApJ*, 511, 885
- Gaensler, B. M., Gotthelf, E. V., & Vasisht, G. 1999, *ApJ*, 526, L37
- Gaensler, B. M., Manchester, R. N., Staveley-Smith, L., Tzioumis, A. K., Reynolds, J. E., & Kesteven, M. J. 1997, *ApJ*, 479, 845
- Gotthelf, E. V., Petre, R., & Hwang, U. 1997, *ApJ*, 487, L175
- Gotthelf, E. V., & Vasisht, G. 1997, *ApJ*, 486, L133
- Gotthelf, E. V., Vasisht, G., Boylan-Kolchin, M., & Torii, K. 2000, *ApJ*, 542, L37
- Gotthelf, E. V., Vasisht, G., & Dotani, T. 1999, *ApJ*, 522, 49
- Gould, A. 1994, *ApJ*, 425, 51
- Hameury, J.-M., Menou, K., Dubus, G., Lasota, J.-P., & Huré, J.-M. 1998, *MNRAS*, 298, 1048
- Harnden, F. R., & Seward, F. D. 1984, *ApJ*, 283, 279

- Harrison, P. A., Lyne, A. G., & Anderson, B. 1993, *MNRAS*, 261, 113
- Heger, A., Langer, N., & Woosley, S. E. 2000, *ApJ*, 528, 368
- Heger, A., Woosley, S. E., & Spruit, H. C. 2004, *astro-ph/0409422*
- Holtzman, J. A., Burrows, C. J., Casertano, S., Hester, J. J., Trauger, J. T., Watson, A. M., & Worthey, G. 1995, *PASP*, 107, 1065
- Houck, J. C., & Chevalier, R. A. 1991, *ApJ*, 376, 234
- Howarth, I. D. 1983, *MNRAS*, 203, 301
- Hurley, K., et al. 2000, *ApJ*, 528, L21
- Illarionov, A. F., & Sunyaev, R. A. 1975, *A&A*, 39, 185
- Jaroszyński, M., Abramowicz, M. A., & Paczyński, B. 1980, *Acta Astronomica*, 30, 1
- Joss, P. C., Podsiadlowski, P., Hsu, J. J. L., & Rappaport, S. 1988, *Nature*, 331, 237
- Kaart, P., et al. 2001, *ApJ*, 321, L29
- Kirshner, R. P., Sonneborn, G., Crenshaw, D. M., & Nassiopoulos, G. E. 1987, *ApJ*, 320, 602
- Koptsevich, A. B., Pavlov, G. G., Zharikov, S. V., Sokolov, V. V., Shibanov, Y. A., & Kurt, V. G. 2001, *A&A*, 370, 1004
- Kozma, C., & Fransson, C. 1998, *ApJ*, 496, 946
- Kristian, J. 1991, *Nature*, 349, 747
- Kristian, J., et al. 1989, *Nature*, 338, 234
- de Loore, C., & Vanbeveren, D. 1992, *A&A*, 260, 273
- Lucy, L. B., Danziger, I. J., Gouiffes, C., & Bouchet, P. 1989, in *Structure & Dynamics of the Interstellar Medium*, IAU Colloq. 120, ed. G. Tenorio-Tagle, M. Mole, & J. Melnick (Berlin: Springer), 164
- Lucy, L. B., Danziger, I. J., Gouiffes, C., & Bouchet, P. 1991, in *Supernovae*, ed. S. E. Woosley (Berlin: Springer), 82
- Lundqvist, P., & Fransson, C. 1996, *ApJ*, 464, 924

- Lundqvist, P., Kozma, C., Sollerman, J., & Fransson, C. 2001, *A&A*, 374, 629
- Lundqvist, P., Sollerman, J., Kozma, C., Larsson, B., Spyromilio, J., Crotts, A. P. S., Danziger, J., & Kunze, D. 1999, *A&A*, 347, 500
- Mack, J. et al. 2003, “ACS Data Handbook,” Version 2.0, (Baltimore: STScI)
- Marsden, D., et al. 1997, *ApJ*, 491, L39
- Marshall, F. E., Gotthelf, E. V., Zhang, W., Middleditch, J., & Wang, Q. D. 1998, *ApJ*, 499, L179
- McCray, R. 1993, *ARA&A*, 31, 175
- Menou, K., Esin, A. A., Narayan, R., Garcia, M. R., Lasota, J.-P., & McClintock, J. E. 1999, *ApJ*, 520, 276
- Menou, K., Perna, R., & Hernquist, L. 2001, *ApJ*, 559, 1032
- Mereghetti, S., Bandiera, R., Bocchino, F., & Israel, G. L. 2002, *ApJ*, 574, 873
- Mereghetti, S., Bignami, G. F., & Caraveo, P. A. 1996, *ApJ*, 464, 842
- Middleditch, J., Pennypacker, C. R., & Burns, M. S. 1987, *ApJ*, 315, 142
- Middleditch, J., et al. 2000, *New Astronomy*, 5, 243
- Mignani, R. P., Pulone, L., Marconi, G., Iannicola, G., & Caraveo, P. A. 2000, *A&A*, 355, 603
- Mitchell, R. C., Baron, E., Branch, D., Hauschildt, P. H., Nugent, P. E., Lundqvist, P., Blinnikov, S., & Pun, C. S. J. 2002, *ApJ*, 574, 293
- Narayan, R., Mahadevan, R., & Quataert, E. 1998, *Theory of Black Hole Accretion Discs*, ed. M. Abramowicz, G. Bjornsson, & J. Pringle (Cambridge: Cambridge Univ. Press)
- Natta, A., & Panagia, N. 1984, *ApJ*, 287, 228
- Nomoto, K., Shigeyama, T., & Hashimoto, M. 1987, in *SN 1987A*, ed. I. J. Danziger (ESO: Garching) p. 325
- Ögelman, H., & Alpar, M. A. 2004, *ApJ*, 603, L33
- Panagia, N. 1999, in *New Views of the Magellanic Cloud*, IAU Symp. 190, ed. Y.-H. Chu, N. Suntzeff, J. Hesser, & D. Bohlender (San Francisco: ASP), 549

- Panagia, N., Gilmozzi, R., Macchetto, F., Adorf, H.-M., & Kirshner, R. P. 1991, *ApJ*, 380, L23
- Panagia, N., Romaniello, M., Scuderi, S., & Kirshner, R. P. 2000, *ApJ*, 539, 197
- Park, S., Zhekov, S. A., Burrows, D. N., Michael, E., McCray, R., Garmire, G. P., & Hasinger, G. 2004, *Advances in Space Research*, 33, 386
- Pavlov, G. G., Stringfellow, G. S., & Cordova, F. A. 1996, *ApJ*, 467, 370
- Pavlov, G. G., Zavlin, V. E., Aschenbach, B., Trümper, J., & Sanwal, D. 2000, *ApJ*, 531, L53
- Pavlov, G. G., Zavlin, V. E., & Sanwal, D. 2002, in *Neutron Stars, Pulsars and Supernova Remnants*, Proc. of the 270-th Heraeus Seminar, ed. W. Becker, H. Lesch & J. Trümper (MPE Report 278), 283 (astro-ph/0206024)
- Pavlov, G. G., Zavlin, V. E., Sanwal, D., & Trümper, J. 2002, *ApJ*, 569, L95
- Perna, R., Hernquist, L. E., & Narayan, R. 2000, *ApJ*, 541, 344
- Petre, R., Becker, C. M., & Winkler, P. F. 1996, *ApJ*, 541, 344
- Podsiadlowski, P. 1989, Ph.D. Thesis, Massachusetts Institute of Technology
- Pringle, J. E. 1974, Ph.D. Thesis, University of Cambridge
- Rho, J., & Petre, R. 1997, *ApJ*, 484, 828
- Sanduleak, N. 1969, *Contr. CTIO*, 89, 1
- Sasaki, M., Plucinsky, P. P., Gaetz, T. J., Smith, R. K., Edgar, R. J., & Slane, P. O. 2004, *ApJ*, 617, 322
- Savage, B. D., & Mathis, J. S. 1979, *ARA&A*, 17, 73
- Scuderi S., Panagia, N., Gilmozzi, R., Challis, P. M., & Kirshner, R. P. 1996, *ApJ*, 465, 956
- Serafimovich, N. I., Shibanov, Yu. A., Lundqvist, P., & Sollerman, J. 2004, *A&A*, 425, 1041
- Seward, F. D., & Harnden, F. R. J. 1994, *ApJ*, 421, 581
- Seward, F. D., Harnden, F. R., & Helfand, D. J. 1984, *ApJ*, 287, L19
- Shakura, N. I., & Sunyaev, R. A. 1973, *A&A*, 24, 337

- Shapiro, S. L., Lightman, A. P., & Eardley, D. M. 1976, *ApJ*, 204, 187
- Shibanov, Y. A., Koptsevich, A. B., Sollerman, J., & Lundqvist, P. 2003, *A&A*, 406, 645
- Shklovskii, I. S. 1979, *Nature*, 279, 703
- Shtykovskiy, P., Lutovinov, A., Gilfanov, M., & Sunyaev, R. 2004, preprint (astro-ph/0411731)
- Soderberg, A. M., Challis, P. M., & Suntzeff, N. B. 1999, *BAAS*, 31, 977
- Sollerman, J., et al. 2000, *ApJ*, 537, 861
- Sonneborn, G., Altner, B., & Kirshner, R. P. 1987, *ApJ*, 323, L35
- Stetson, P. 1987, *PASP*, 99, 191
- Suntzeff, N. B., & Bouchet, P. 1990, *AJ*, 99, 650
- Suntzeff, N. B., Phillips, M. M., Elias, J. H., DePoy, D. L., & Walker, A. R. 1992, *ApJ*, 384, L33
- Tananbaum, H. 1999, *IAU Circ.*, No. 7246
- Thorsett, S. E. 1992, *Nature*, 356, 690
- Torii, K. I., Kinugasa, K., Toneri, T., Asanuma, T., Tsunemi, H., Dotani, T., Mitsuda, K., Gotthelf, E. V., & Petre, R. 1998, *ApJ*, 494, L207
- Torii, K. I., Kinugasa, K., Katayama, K., Tsunemi, H., & Yamauchi, S. 1998, *ApJ*, 503, 843
- Tuohy, I., & Garmire, G. 1980, *ApJ*, 239, 107
- van den Bergh, S., & Kamper, K. W. 1983, *ApJ*, 268, 129
- Vasisht, G., Kulkarni, S. R., Frail, D. A., & Greiner, J. 1994, *ApJ*, 431, L35
- Walborn, N. R., Lasker, B. M., Laidler, V. G., & Chu, Y.-H. 1987, *ApJ*, 321, L41
- Wang, L., et al. 1996, *ApJ*, 466, 998
- Wang, L., et al. 2002, *ApJ*, 579, 671
- Wang, Z.-X., & Chakrabarty, D. 2002, in *Neutron Stars in Supernova Remnants*, ASP Conf. Series Vo. 271, ed. P. O. Slane & B. M. Gaensler (San Francisco: ASP), 297 (astro-ph/0112125)

- Wang, Q. D., & Gotthelf, E. V. 1998, *ApJ*, 509, L109
- West, R. M. 1987, *A&A*, 177, L1
- White, G. L., & Malin, D. F. 1987, *Nature*, 327, 36
- Winkler, P. F., & Kirshner, R. P. 1985, *ApJ*, 299, 981
- Winkler, P. F., Kirshner, R. P., & Irwin, M. M. 1986, *BAAS*, 18, 1053
- Woods, P. M., Kouveliotou, C., van Paradijs, J., Finger, M. H., & Thompson, C. 1999, *ApJ*, 518, L103
- Woosley, S. E. 1998, *ApJ*, 330, 218
- Zampieri, L., Colpi, M., Shapiro, S. L., & Wasserman, I. 1998, *ApJ*, 505, 876
- Zavlin, V. E., & Pavlov, G. G. 2004, in *Proc. of the XMM-Newton EPIC Consortium*, *Mem.S.A.It.*, 75, 458 (astro-ph/0312326)
- Zavlin, V. E., & Pavlov, G. G. 2004, *ApJ*, 616, 452

Table 1. STIS Data.

Grating	Slit	Exposure Time (s)	Wavelength Range (Å)
G140L	0.5''	10400	1140–1730
G230L	0.5''	10400	1568–3184
G430L	0.2''	7800	2900–5700
G750L	0.2''	7800	5236–10266

Table 2. ACS Imaging Data.

ACS/HRC Filter	Band	Exposure Time (s)	Pivot Wavelength (Å)	RMS Bandwidth (Å)
F330W	HRC UV	400	3362.7	1738.2
F435W	Johnson B	400	4311.0	3096.8
F555W	Johnson V	200	5355.9	3571.9
F625W	SDSS r	200	6295.5	4153.1
F814W	Broad I	200	8115.3	7034.5

Table 3. Limits From ACS Images.

Filter	Flux Limit of 4-pixel Aperture (counts)	Flux Limit of Infinite Aperture (counts)	Effective F_λ (10^{-18} ergs $\text{s}^{-1} \text{cm}^{-2} \text{\AA}^{-1}$)	Applied Filter Width (\AA)	L (10^{32} ergs s^{-1})	L (L_\odot)
F330W	0.51	0.71	3.97	2900–3690	9.96	0.26
F435W	2.55	3.27	3.59	3690–4800	12.7	0.33
F555W	2.93	3.80	1.99	4800–5700	5.96	0.15
F625W	6.62	8.67	2.70	5700–7050	11.6	0.30
F814W	4.86	7.61	1.32	7050–9650	10.9	0.28

Table 4. Comparison with Point Sources in Other SNRs

SNR	Source	$\log L_X$ (ergs s ⁻¹)	$\log L_{opt}$ (ergs s ⁻¹)	Age (yr)	Possible in SN 1987A?	Reference
SN 1987A	Point source	≤ 33.74	≤ 33.9	16.75		1,2
Young Pulsars						
Kes 75	PSR J1846-0258	> 34.6	...	1700	N	3* , 27
Crab	PSR B0531+21	36.2	33.8	950	N	4, 5 [†] , 28
N158A	PSR B0540-69	36.4	33.9	1660	N	6, 7 [†] , 30
N157B	PSR J0537-6910	35.5	≤ 33.1	5000	N	8* , 25, 31
MSH 15-52	PSR B1509-58	35.3	...	1800	N	9* , 32
Vela	PSR B0833-45	31.3	28.8	1.1×10^4	Y	4, 10 [†] , 29
Monogem Ring	PSR B0656+14	30.2	28.2	1.1×10^5	Y	4, 11-13 [†] , 29
Geminga	PSR J0633+1746	30.2	27.5	3.4×10^5	Y	4, 11, 13 [†] , 29
Nonplerionic X-Ray Point Sources in SNRs						
Cas A	Point source	33.8-34.6/33.3 ^a	$\leq 29.1^{\ddagger}$	400	N/Y	14* , 26, 34
Pup A	1E 0820-4247	33.6 ^b	$\leq 30.3^{\ddagger}$	3000	Y	15* , 27, 33
RCW 103	1E 1614-5055	33.9 ^b	$\leq 30.8^{\ddagger}$	8000	N	16* , 27, 35
PKS 1209-52	1E 1207-5209	33.1 ^b	$\leq 30.1^{\ddagger}$	7000	Y	17, 18* , 27, 36
Anomalous X-ray Pulsars						
Kes 73	1E 1841-045	35.5	...	≤ 2000	N	19* , 37
G29.6+0.1	AX J1845-0258	38.6/34.9 ^a	...	≤ 8000	N	20* , 38
CTB 109	1E 2259+586	36.9 ^c	...	8800	N	21* , 39
Soft Gamma Repeaters						
G42.8+0.6?	SGR 1900+14	34.6 ^c	...	10^4	N	22* , 40
G337.0-0.1?	SGR 1627-41	35.8	...	5000	N	23, 24*

Note. — X-ray luminosities are in the 1-10 keV band. All X-ray luminosities $\log L_X$ are for power law sources, except as noted.

^aX-ray data can be fit by either a power law or a blackbody source, shown $\log L_{pl}/\log L_{bb}$.

^bX-ray luminosity is for a blackbody source.

^cX-ray luminosity includes contributions from both power law and blackbody models.

*Taken from Table 3 in Chakrabarty et al. (2001).

[†]Taken from Table 2 in Zavlin & Pavlov (2004b).

[‡]Optical upper limits were computed from *R*-band limiting magnitudes (Johnson *R* in the case of Cas A, SDSS *r* in the case of Pup A, RCW 103, & PKS 1209-52). An optical power law spectrum was assumed with a negative

spectral index $\alpha = -1.07$, based on the optical spectrum of PSR B0540-69 (Serafimovich et al. 2004), and integrated over the wavelength range 2900–9650Å.

References. — (1) Park et al. 2004. (2) This paper. (3) Gotthelf et al. 2000. (4) Zavlin & Pavlov 2004b. (5) Sollerman et al. 2000. (6) Kaart et al. 2001. (7) Middleditch, Pennypacker, & Burns 1987. (8) Wang & Gotthelf 1998. (9) Marsden et al. 1997. (10) Shibanov et al. 2003. (11) Zavlin & Pavlov 2004a. (12) Pavlov, Zavlin, & Sanwal 2002. (13) Koptsevich et al. 2001. (14) Chakrabarty et al. 2001. (15) Petre, Becker, & Winkler 1996. (16) Mereghetti, Bignami, & Caraveo 1996. (17) Tuohy & Garmire 1980. (18) Gotthelf, Petre, & Hwang 1997. (19) Gotthelf, Vasisht, & Dotani 1999. (20) Torii et al. 1998. (21) Rho & Petre 1997. (22) Woods et al. 1999. (23) Corbel et al. 1999. (24) Hurley et al. 2000. (25) Fesen et al. 2002. (26) Wang & Chakrabarty 2002. (27) Mignani et al. 2000. (28) Mereghetti et al. 2002. (29) Pavlov, Stringfellow, & Cordova 1996. (30) Seward, Harnden, & Helfand 1984. (31) Marshall et al. 1998. (32) Thorsett 1992. (33) Winkler, Kirshner, & Irwin 1986. (34) van den Bergh & Kamper 1983. (35) Torii et al. 1998. (36) Pavlov et al. 2002. (37) Gotthelf & Vasisht 1997. (38) Gaensler, Gotthelf, & Vasisht 1999. (39) Sasaki et al. 2004. (40) Vasisht et al. 1994.

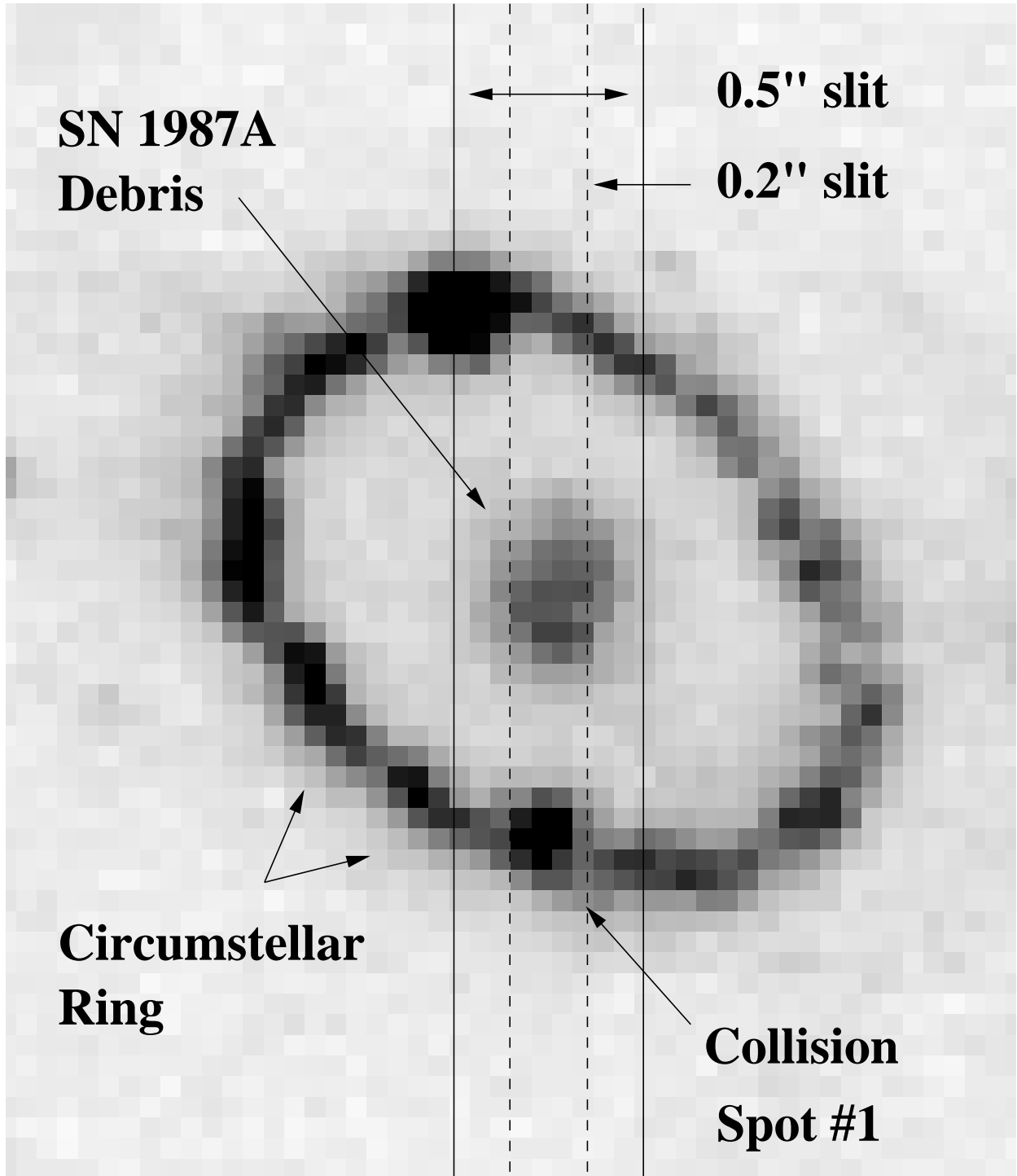


Fig. 1.— *STIS* slit positions for 1999 spectral data include the central debris and portions of the circumstellar ring. The 0.5" slit was used for the UV spectrum and the 0.2" slit was used for the optical spectrum (see Table 1).

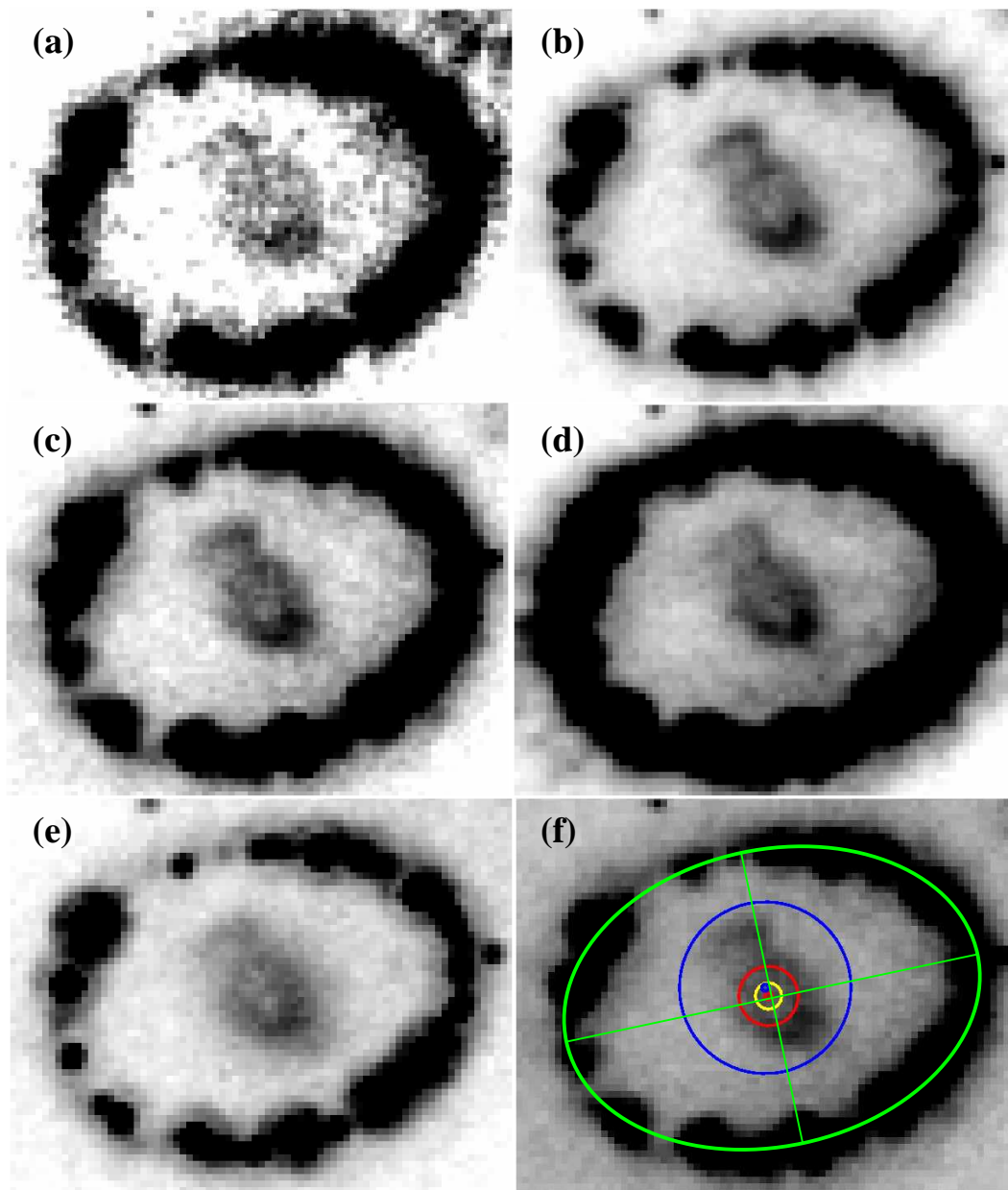


Fig. 2.— *ACS/HRC* images of SN 1987A in five filters: (a) *HRC* UV - F330W, (b) Johnson B - F435W, (c) Johnson V - F555W, (d) SDSS r - F625W, and (e) Broad I - F814W. No central point source is detected in any band. Part (f) shows the F555W image with three determinations of the center of the debris: by eye (red dot), by fitting a circle to the central debris (blue), and by fitting an ellipse to the inner ring of the SNR (green). The yellow circle has a radius of two pixels and shows the uncertainty in determining the centerpoint. The red circle has a radius of 4.5 pixels and encloses the maximum distance that a compact object may have travelled from the center, with a kick velocity ≤ 1000 km/s.

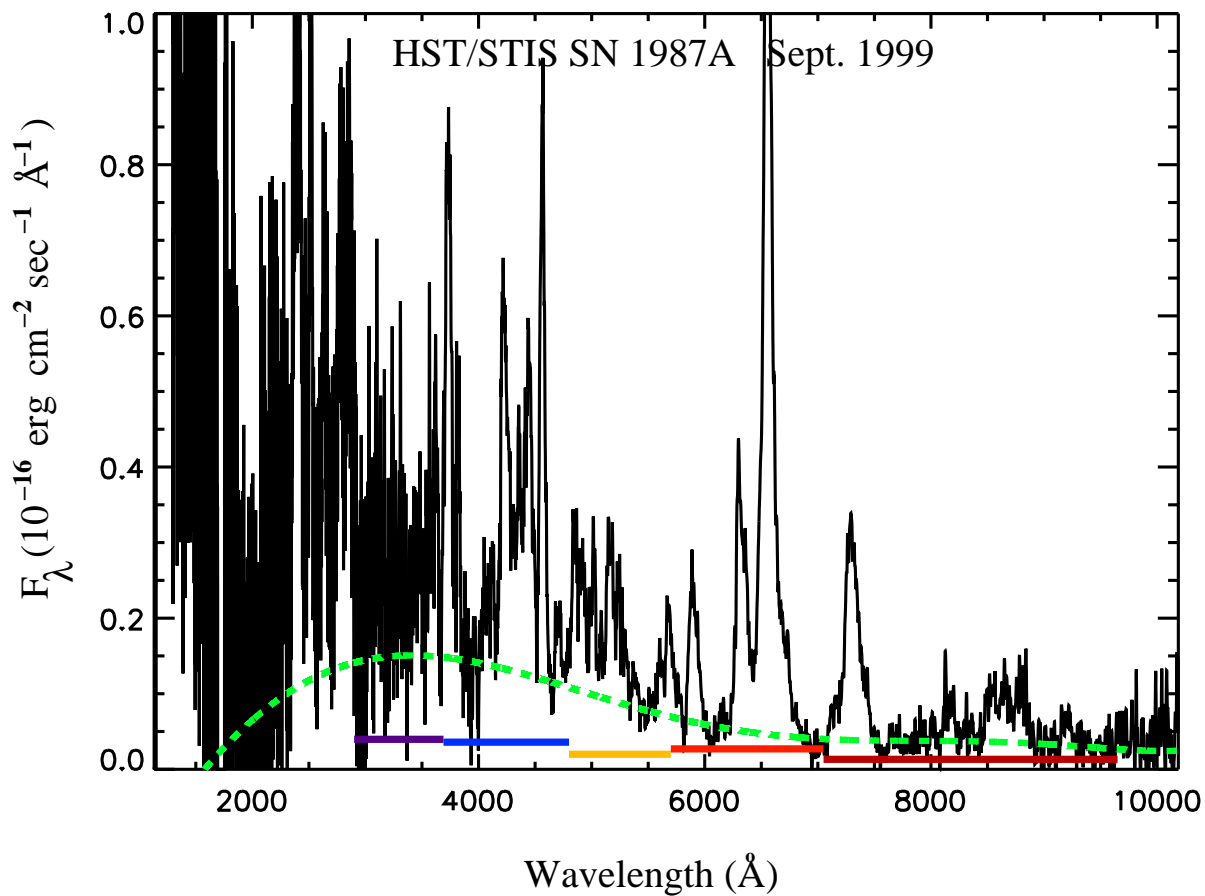


Fig. 3.— The 1999 September spectrum of SN 1987A, corrected for interstellar extinction. The fit to a possible underlying continuum is shown as the green dashed line. Also shown are the 2003 November *ACS/HRC* limits, plotted as horizontal colored bars that span the applied filter width. From left to right, these are the F330W, F435W, F555W, F625W, and F814W filter bands. The imaging data place a more stringent limit on a continuum point source in the remnant than do the spectral data.

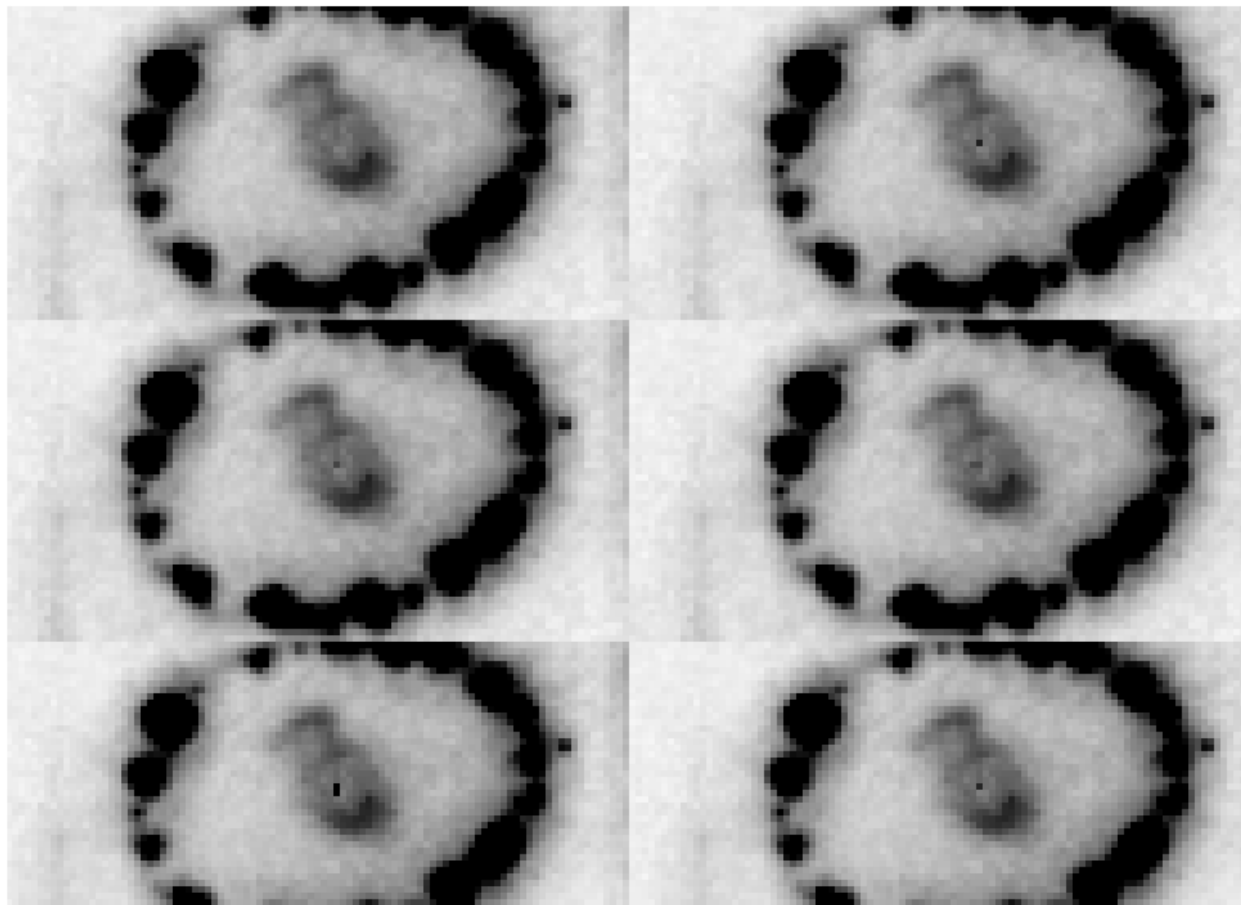


Fig. 4.— *ACS/HRC* image of SN 1987A in the Johnson B filter (F435W) with inserted point sources. The inserted sources increase in total counts from left to right and top to bottom. The top left inserted source is not easily detectable, and is therefore the upper limit in the B-band.

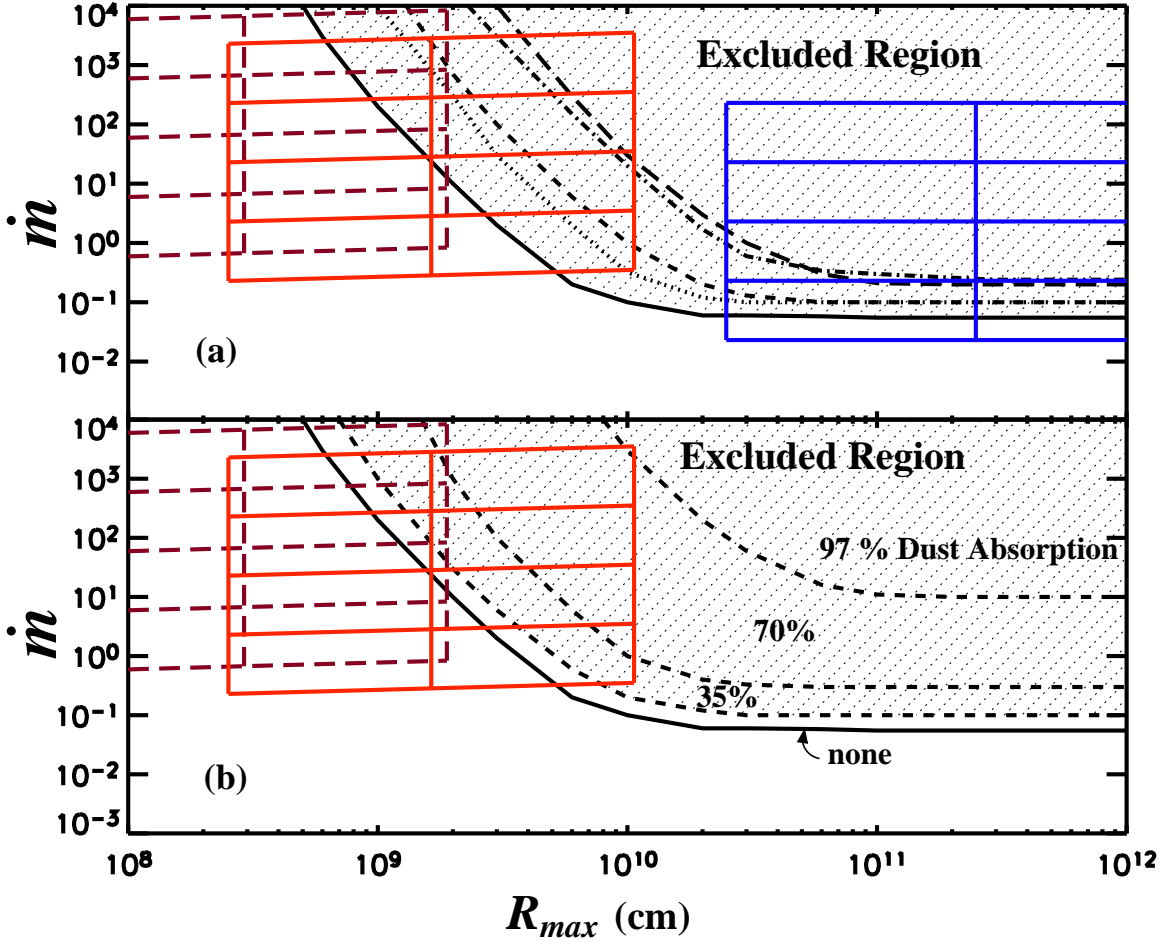


Fig. 5.— Constraints on thin disk accretion rate and disk radius given by our observed upper limit. (a) The solid line shows the limit imposed by the UV observations. The shaded region shows disk radii and accretion rates that are excluded by the observed limit on counts in the UV. Limits from other bands are also shown: the dotted, short-dashed, dot-dashed, and long-dashed lines correspond to the limits from the B-band, V-band, R-band, and I-band, respectively. The blue grid shows accretion disks predicted by the PHN fallback model. The red grids show the accretion disks predicted by the MPH fallback model; the solid grid shows the results for hot disks ($T = 10^6$ K), while the darker dashed grid shows the results for cooler disks ($T = 10^4$ K). In each grid, vertical lines correspond to initial disk radii (from left to right) of 10^6 cm, 10^7 cm, and 10^8 cm. Horizontal lines correspond to initial disk masses (from top to bottom) of $10^{-1}M_{\odot}$, $10^{-2}M_{\odot}$, $10^{-3}M_{\odot}$, $10^{-4}M_{\odot}$, and $10^{-5}M_{\odot}$. (b) The effect of dust absorption on the upper limit. As in (a), the solid curve is the UV-band limit. The dashed lines show the UV-band limit in the case of 35%, 70%, and 97% dust absorption within the remnant. The red grids show the accretion disks predicted by the MPH fallback model, as in (a).